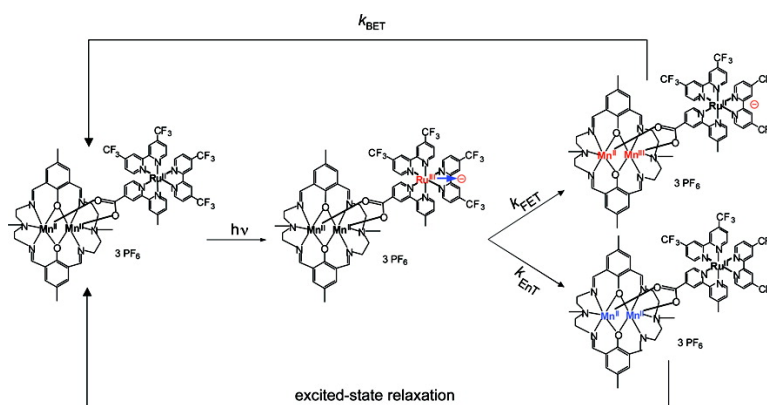Article

Distinguishing between Dexter and Rapid Sequential Electron Transfer in Covalently Linked Donor−Acceptor Assemblies

Monica Soler, and James K. McCusker

More About This Article

Additional resources and features associated with this article are available within the HTML version:

- Supporting Information
- Links to the 2 articles that cite this article, as of the time of this article download
- Access to high resolution figures
- Links to articles and content related to this article
- Copyright permission to reproduce figures and/or text from this article

View the Full Text HTML

Distinguishing between Dexter and Rapid Sequential Electron Transfer in Covalently Linked Donor−Acceptor Assemblies

Monica Soler and James K. McCusker*

Department of Chemistry, Michigan State University, East Lansing, Michigan 48824

Received September 13, 2007; E-mail: jkm@chemistry.msu.edu

Abstract: The syntheses, physical, and photophysical properties of a family of complexes having the general formula $[M_2(L)(mcb)(Ru(4,4'-(X)_2-bpy)_2)](PF_6)_3$ (where $M = Mn^{II}$ or Zn^{II}, $X = CH_3$ or CF_3, mcb is 4′-methyl-4-carboxy-2,2′-bipyridine, and L is a Schiff base macrocycle derived from 2,6-diformyl-4-methylphenol and bis(2-aminoethyl)-*N*-methylamine) are described. The isostructural molecules all consist of dinuclear metal cores covalently linked to a Ru^{II} polypyridyl complex. Photoexcitation of $[Mn_2(L)(mcb)(Ru((CF_3)_2-bpy)_2)]$-$(PF_6)_3$ (**4**) in deoxygenated CH_2Cl_2 solution results in emission characteristic of the ^{3}MLCT excited state of the Ru^{II} chromophore but with a lifetime ($\tau_{obs} = 5.0 \pm 0.1$ ns) and radiative quantum yield ($\Phi_r \approx 7 \times 10^{-4}$) that are significantly attenuated relative to the Zn^{II} model complex $[Zn_2(L)(mcb)(Ru((CF_3)_2-bpy)_2)](PF_6)_3$ (**6**) ($\tau_{obs} = 730 \pm 30$ ns and $\Phi_r = 0.024$, respectively). Quenching of the ^{3}MLCT excited state is even more extensive in the case of $[Mn_2(L)(mcb)(Ru((CH_3)_2-bpy)_2)](PF_6)_3$ (**3**), whose measured lifetime ($\tau_{obs} = 45 \pm 5$ ps) is $>10^4$ shorter than the corresponding model complex $[Zn_2(L)(mcb)(Ru((CH_3)_2-bpy)_2)](PF_6)_3$ (**5**) ($\tau_{obs} = 1.31 \pm 0.05$ μs). Time-resolved absorption measurements on both Mn-containing complexes at room-temperature revealed kinetics that were independent of probe wavelength; no spectroscopic signatures for electron-transfer photoproducts were observed. Time-resolved emission data for complex **4** acquired in CH_2Cl_2 solution over a range of 200−300 K could be fit to an expression of the form $k_{nr} = k_0 + A \cdot \exp\{-\Delta E/k_B T\}$ with $k_0 = 1.065 \pm 0.05 \times 10^7$ s^{-1}, $A = 3.7 \pm 0.5 \times 10^{10}$ s^{-1}, and $\Delta E = 1230 \pm 30$ cm^{-1}. Assuming an electron-transfer mechanism, the variable-temperature data on complex **4** would require a reorganization energy of $\lambda \sim 0.4-0.5$ eV which is too small to be associated with charge separation in this system. This result coupled with the lack of enhanced emission at temperatures below the glass-to-fluid transition of the solvent and the absence of visible absorption features associated with the Mn^{II}_2 core allows for a definitive assignment of Dexter transfer as the dominant excited-state reaction pathway. A similar conclusion was reached for complex **3** based in part on the smaller driving force for electron transfer ($\Delta G_0^{ET} = -0.1$ eV), the increase in probability of Dexter transfer due to the closer proximity of the donor excited state to the dimanganese acceptor, and a lack of emission from the compound upon formation of an optical glass at 80 K. Electronic coupling constants for Dexter transfer were determined to be ~ 10 cm^{-1} and ~ 0.15 cm^{-1} in complexes **3** and **4**, respectively, indicating that the change in spatial localization of the excited state from the bridge (complex **3**) to the periphery of the chromophore (complex **4**) results in a decrease in electronic coupling to the dimanganese core of nearly 2 orders of magnitude. In addition to providing insight into the influence of donor/acceptor proximity on exchange energy transfer, this study underscores the utility of variable-temperature measurements in cases where Dexter and electron-transfer mechanisms can lead to indistinguishable spectroscopic observables.

Introduction

The study of photoinduced electron and energy-transfer processes represents an extremely active area of chemical research.[1] The relevance of such reactions for understanding naturally occurring processes (e.g., photosynthesis)[2] as well as their potential use in the design of nanoscale devices capable of performing a variety of light-induced functions[3] has provided fertile ground for the development of this field over the past two decades. In recent years, considerable attention has been paid to the preparation and characterization of covalently linked assemblies for the study of the donor/acceptor interactions that form the basis of photoreactivity in molecular systems.[4] The

(1) For information on issues pertaining to solar energy conversion see: "Basic Research Needs for Solar Energy Utilization", Office of Basic Energy Science, U.S. Department of Energy, Washington, D.C., 2005 (available on the U.S. Department of Energy website).

(2) (a) Wasielewski, M. R. *Chem. Rev.* **1992**, *92*, 435−461. (b) Gust, D.; Moore, T. A.; Moore, A. L. *Acc. Chem. Res.* **2001**, *34*, 40−48. (c) Lomoth, R.; Maguson, A.; Sjodin, M.; Huang, P.; Styring, S.; Hammarstrom, L. *Photosynth. Res.* **2006**, *87*, 25−40, and references therein. (d) Alstrum-Acevedo, J. H.; Brennaman, M. K.; Meyer, T. J. *Inorg. Chem.* **2005**, *44*, 6802−6827.

(3) (a) Hagfeldt, A.; Grätzel, M. *Acc. Chem. Res.* **2000**, 33, 269−277. (b) Collin, J.-P.; Gaviña, P.; Heitz, V.; Sauvage, J.-P. *Eur. J. Inorg. Chem.* **1998**, 1−14. (c) Salman, H.; Eichen, Y.; Speiser, S. *Mater. Sci. Eng., C* **2006**, *26*, 881−885. (d) Wiess, E. A.; Wasielewski, M. R.; Ratner, M. A. *Top. Curr. Chem.* **2005**, *257*, 103−133. (e) Guldi, D. M. *Phys. Chem. Chem. Phys.* **2007**, *9*, 1400−1420. (f) Balzani, V. *Photochem. Photobiol. Sci.* **2003**, *2*, 459−476, and references therein. (g) Guo, F.; Ogawa, K.; Kim, Y.-G.; Danilov, E. O.; Castellano, F. N.; Reynolds, J. R.; Schanze, K. S. *Phys. Chem. Chem. Phys.* **2007**, *9*, 2724−2734, and references therein. (h) Guldi, D. M.; Rahman, A.; Sgobba, V.; Ehil, C. *Chem. Soc. Rev.* **2006**, *35*, 471−487.

inherent advantage of this structural motif in terms of circumventing diffusion-limited reaction chemistry has resulted in the elucidation of details concerning, for example, the Marcus inverted region[5] and the role of bridge energetics in studies of long-range electron and energy transfer.[6] Inorganic charge-transfer complexes—particularly d[6] metal complexes of Ru, Os, Re, and Ir—have been particularly useful in such studies due in part to their long-lived emissive excited states as well as an inherent versatility vis-à-vis their ability to act as either a donor or an acceptor in both classes of reactions.[7]

An unfortunate consequence of this versatility is that determination of the mechanism of excited-state reactivity often proves to be a difficult problem;[8] which pathway(s) will be operative in any given case will depend on a variety of factors including the electronic structures of the constituents and the degree and nature of electronic communication between the donor and the acceptor. Electron transfer is a through-bond mechanism that is driven largely by a balance between the thermodynamics of the donor/acceptor pair and the structural changes accompanying the redox reaction.[9] Electron transfer can occur between species in intimate contact or at distances in excess of 30 Å as shown by the seminal studies of Gray and co-workers.[10] Energy transfer, which involves deactivation of an electronic excited of the donor and concomitant formation of an excited state of the acceptor, can occur via through-space (Förster) or through-bond (Dexter) mechanisms.[11] The dipolar
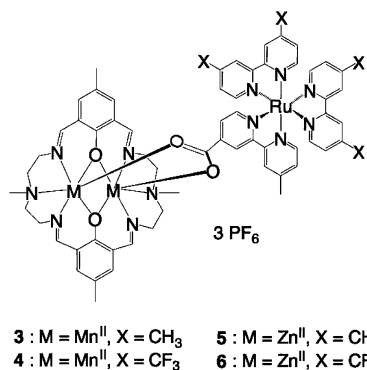
nature of Förster transfer[12] gives rise to a rate that falls off as r^6 and can be operative up to 100 Å away, whereas the exchange-based Dexter mechanism has a much steeper exponential dependence on distance due to its reliance on orbital overlap.[13] In covalently linked systems with a favorable driving force for electron transfer, all three of these pathways are potentially active.

The gold standard for establishing an electron-transfer mechanism is direct observation of the charge-separated species (i.e., spectroscopic and/or chemical evidence of the oxidized donor and/or the reduced acceptor); however, circumstances can easily arise for which this is not possible. For example, the photoproducts might be characterized by very weak absorption features, or, as we will be considering in this paper, the parameters governing the forward- and back-electron-transfer reactions may be such that an insufficient concentration of product would be formed to allow for detection. Energy transfer can be equally problematic for systems in which the acceptor is nonemissive. The availability of an analytical expression for the rate of Förster transfer coupled with its dependence on spectral overlap between the emission of the donor and absorption(s) of the acceptor significantly simplifies establishing the viability of this mechanism. The net result of Dexter transfer is identical to the Förster mechanism but does not require significant oscillator strength on the part of the acceptor; because of this, Dexter transfer can be operative in a wider array of chemical systems but can be more difficult to unequivocally establish.[14] As a result, Dexter transfer is often the default mechanism invoked in systems containing weakly absorbing acceptors for which a charge-separated species is not detected. In a sense this represents the lead standard for photophysical characterization, but in many of these cases few other options are usually available.

One challenge in this area of research, then, is to develop well-characterized systems that allow for an unambiguous determination of the mechanism of reactivity. Recent research efforts in our group have focused on the study of intramolecular electron and energy-transfer processes involving polynuclear transition-metal complexes in an effort to understand how modulations in their electronic structure affect reactivity.[15] Within this context, we have developed a donor—acceptor assembly consisting of a spin-coupled dinuclear core covalently bound to a Ru[II] polypyridyl chromophore (Scheme 1) that provides an interesting opportunity to explore some of the mechanistic issues described above as it relates to excited-state dynamics. The advantage of this system in terms of the

(4) (a) Balzani, V.; Bergamini, G.; Marchioni, F.; Ceroni, P. *Coord. Chem. Rev.* **2006**, *250*, 1254−1266. (b) Sun, S. S.; Lees, A. J. *Coord. Chem. Rev.* **2002**, *230*, 171−192. (c) Goldsmith, R. H.; Wasielewski, M. R.; Ratner, M. A. *J. Phys. Chem. B* **2006**, *110*, 20258−20262. (d) Ward, M. D.; Barigelletti, F. *Coord. Chem. Rev.* **2001**, *216*, 127. See also ref 14a.

(5) (a) Miller, J. R.; Calcaterra, L. T.; Closs, G. L. *J. Am. Chem. Soc.* **1984**, *106*, 3047−3049. (b) Closs, G. L.; Miller, J. R. *Science* **1988**, *240*, 440−447. (c) Liang, N.; Miller, J. R.; Closs, G. L. *J. Am. Chem. Soc.* **1990**, *112*, 5353−5354. (d) Ratera, I.; Sporer, C.; Ruiz-Molina, D.; Ventosa, N.; Baggerman, J.; Brouwer, A. M.; Rovira, C.; Veciana, J. *J. Am. Chem. Soc.* **2007**, *129*, 6117−6129. (e) Kang, Y. K.; Duncan, T. V.; Therien, M. J. *J. Phys. Chem. B* **2007**, *111*, 6829−6838. (f) Nicolet, O.; Banerji, N.; Pages, S.; Vauthey, E. *J. Phys. Chem. A* **2005**, *109*, 8236−8245. (g) Serron, S. A.; Aldridge, W. S.; Fleming, C. N.; Danell, R. M.; Baik, M. H.; Sykora, M.; Dattelbaum, D. M.; Meyer, T. J. *J. Am. Chem. Soc.* **2004**, *126*, 14506−14514. (h) Chen, P.-Y.; Duesing, R.; Graff, D. K.; Meyer, T. J. *J. Phys. Chem.* **1991**, *95*, 5850−5858.

(6) (a) Weiss, E. A.; Tauber, M. J.; Kelley, R. F.; Ahrens, M. J.; Ratner, M. A.; Wasielewski, M. R. *J. Am. Chem. Soc.* **2005**, *127*, 11842−11850, and references therein. (b) Goldsmith, R. H.; Sinks, L. E.; Kelley, R. F.; Betzen, L. J.; Liu, W. H.; Weiss, E. A.; Ratner, M. A.; Wasielewski, M. R. *Proc. Natl. Acad. Sci. U.S.A.* **2005**, *102*, 3540−3545. (c) Chen, K. Y.; Hsieh, C. C.; Cheng, Y. M.; Lai, C. H.; Chou, P. T.; Chow, T. J. *J. Phys. Chem. A* **2006**, *110*, 12136−12144. (d) Winters, M. U.; Pettersson, K.; Martensson, J.; Albinsson, B. *Chem. Eur. J.* **2005**, *11*, 562−573. (e) Davis, W. B.; Ratner, M. A.; Wasielwski, M. R. *J. Am. Chem. Soc.* **2001**, *123*, 7877−7886.

(7) (a) Vlcek, A.; Busby, M. *Coord. Chem. Rev.* **2006**, *250*, 1755−1762. (b) Chiorboli, C.; Indelli, M. T.; Scandola, F. *Top. Curr. Chem.* **2005**, *257*, 63−102, and references therein. (c) Juris, A.; Manfrin, M. F.; Maestri, M.; Serpone, N. *Inorg. Chem.* **1978**, *17*, 2258. (d) Benniston, A. C.; Harriman, A.; Li, P. Y.; Sams, C. A. *J. Am. Chem. Soc.* **2005**, *127*, 2553−2564.

(8) (a) Borgström, M.; Shaikh, N.; Johansson, O.; Anderlund, M. F.; Styring, S.; Akermark, B.; Magnuson, A.; Hammarström, L. *J. Am. Chem. Soc.* **2005**, *127*, 17504−17515. (b) Abrahamsson, M. L. A.; Baudin, H. B.; Tran, A.; Philouze, C.; Berg, K. E.; Raymond-Johansson, M. K.; Sun, L.; Akermark, B.; Styring, S.; Hammarström, L. *Inorg. Chem.* **2002**, *41*, 1534−1544. (c) Monnereau, C.; Gomez, J.; Blart, E.; Odobel, F.; Wallin, S.; Fallberg, A.; Hammarström, L. *Inorg. Chem.* **2005**, *44*, 4806−4817. (d) Ghanem, R.; Xu, Y.; Pan, J.; Hoffmann, T.; Andersson, J.; Polivka, T.; Pascher, T.; Styring, S.; Sun, L.; Sundstrom, V. *Inorg. Chem.* **2002**, *41*, 6258−6266. (e) Puntoriero, F.; Nastasi, F.; Cavazzini, M.; Quici, S.; Campagna, S. *Coord. Chem. Rev.* **2007**, *251*, 536−545, and references therein. (f) Thompson, A. L.; Gaab, K. M.; Xu, J. J.; Bardeen, C. J.; Martinez, T. J. *J. Phys. Chem. A* **2004**, *108*, 671−682.

(9) For excellent reviews of this topic, see: (a) Barbara, P. F.; Meyer, T. J.; Ratner, M. A. *J. Phys. Chem.* **1996**, *100*, 13148−13168. (b) Marcus, R. A.; Sutin, N. *Biochim. Biophys. Acta* **1985**, *811*, 265−322.

(10) Gray, H. B.; Winkler, J. R. *Proc. Natl. Acad. Sci U.S.A.* **2005**, *102*, 3534−3539, and references therein.

(11) (a) Speiser, S. *Chem. Rev.* **1996**, *96*, 1953−1976. (b) Scandola, F.; Balzani, V. *J. Chem. Educ.* **1983**, *60*, 814−823.

(12) (a) Förster, T. *Discuss. Faraday Soc.* **1959**, *27*, 7. (b) Van Der Meer, B. W.; Coker, G. I.; Chen, S.-Y. *Resonance Energy Transfer Theory and Data*; VCH Publishers: New York, 1994. (c) Scholes, G. D. *Ann. Rev. Phys. Chem.* **2003**, *54*, 57−87.

(13) (a) Dexter, D. L. *J. Chem. Phys.* **1953**, *21*, 836−850. (b) Balzani, V.; Bolletta, F.; Scandola, F. *J. Am. Chem. Soc.* **1980**, *2152−2163*.

(14) For examples, see: (a) Welter, S.; Salluce, N.; Belser, P.; Groeneveld, M.; De Cola, L. *Coord. Chem. Rev.* **2005**, *249*, 1360−1371. (b) Ott, S.; Borgstrom, M.; Hammarström, L.; Johansson, O. *Dalton Trans.* **2006**, *1434−1443*. (c) Brown, W. R.; O'Boyle, N. M.; McHarvey, J. J.; Vos, J. G. *Chem. Soc. Rev.* **2005**, *34*, 641. (d) Barigelletti, F.; Flamigni, L.; Balzani, V.; Collin, J.-P.; Sauvage, J.-P.; Sour, A.; Constable, E. C.; Cargill Thompson, A. M. W. *J. Am. Chem. Soc.* **1994**, *116*, 7692. (e) Goeb, S.; De Nicola, A.; Ziessel, R.; Sabatini, C.; Barbieri, A.; Barigelletti, F. *Inorg. Chem.* **2006**, *45*, 1173. (f) Yeow, E. K. L.; Ziolek, M.; Karolczak, J.; Shevyakov, S. V.; Asato, A. E.; Maciejewski, A.; Steer, R. P. *J. Phys. Chem. A* **2004**, *108*, 10980−10988. See also ref 52a.

(15) (a) Weldon, B. T.; Wheeler, D. E.; Kirby, J. P.; McCusker, J. K. *Inorg. Chem.* **2001**, *40*, 6802−6812. (b) Picraux, L. B.; Smeigh, A. L.; Guo, D.; McCusker, J. K. *Inorg. Chem.* **2005**, *44*, 7849−7856.

Scheme 1

3 : M = Mn^{II}, X = CH$_3$ **5** : M = Zn^{II}, X = CH$_3$
4 : M = Mn^{II}, X = CF$_3$ **6** : M = Zn^{II}, X = CF$_3$

preceding discussion is the chemical tunability inherent in this platform. The complexes of interest are based on Mn^{II}, whose absorptive and electrochemical properties serve to limit the possible modes of reactivity in which this system can engage. Moreover, we can take advantage of substituent effects on the bipyridyl ligands of the Ru^{II} chromophore to manipulate the spatial disposition of the reactive charge-transfer excited state formed upon photoexcitation.[4a] This motif also provides us with the ability to study isostructural analogs in which the Mn^{II} ions are replaced by Zn^{II}, thereby allowing for characterization of the photophysical properties of the chromophore in the absence of excited-state reactivity with the dinuclear core. The syntheses, physical, and photophysical properties of this system are described herein. The confluence of data we have acquired—in particular the use of variable-temperature steady-state and time-resolved spectroscopies—allows us to clearly define excited-state reaction pathways in a donor/acceptor system for which various mechanistic possibilities can, under certain circumstances, lead to identical experimental results.

Experimental Section

General. All reagents were obtained from commercial sources and used without further purification. Solvents were purchased from either Aldrich Chemical Co. or Fisher Scientific and distilled and degassed prior to use. The ligands 4′-methyl-2,2′-bipyridine-4-carboxylic acid {mcb},[16] 4,4′-bis(trifluoromethyl)-2,2′-bipyridine {(CF$_3$)$_2$-bpy},[17] 4,4′-bis(methyl)-2,2′-bipyridine {(CH$_3$)$_2$-bpy},[18] and 2,6-diformyl-4-methylphenol[19] and the complexes Ru((CH$_3$)$_2$-bpy)$_2$Cl$_2$[20] and Ru((CF$_3$)$_2$-bpy)$_2$Cl$_2$[21] were prepared by literature methods. Sodium 4′-methyl-2,2′-bipyridine-4-carboxylate (mcbNa) was obtained by addition of NaOH$_{(aq)}$ to an aqueous solution of 4′-methyl-2,2′-bipyridine-4-carboxylic acid. Elemental analyses were obtained through the analytical facilities at Michigan State University. The electrospray ionization mass spectrometry (ESI-MS) data were acquired by Dr. M. Walla of the University of South Carolina. ^{1}H NMR spectra were recorded on either a Varian 300 MHz or 500 MHz spectrometer. Infrared spectra (4000−400 cm^{-1}) were measured as KBr pellets using a Mattson Galaxy series 3000 FTIR spectrophotometer.

[Mn$_2$(L)(mcb)](PF$_6$) (1). Complex **1** was synthesized by the reaction of a dimanganese(II) precursor, [Mn$_2$LCl]$^+$, and mcbNa.

[Mn$_2$(L)Cl](PF$_6$). This molecule was obtained by a modified version of a previously reported synthesis.[22] *N,N*-Bis(2-aminoethyl)-*N*-methyl-amine (0.360 g, 3.07 mmol) and 2,6-diformyl-4-methylphenol (0.504 g, 3.07 mmol) were dissolved in a minimum amount of ethanol and stirred for 30 min under a N$_2$ atmosphere. Addition of an ethanol solution of MnCl$_2$·4H$_2$O (0.608 g, 3.07 mmol) resulted in the formation of an orange precipitate, which redissolved upon addition of NEt$_3$ (0.311 g, 3.07 mmol). The reaction was stirred with gentle heating for an additional 30 min. Addition of NBu$_4$PF$_6$ (0.892 g, 2.30 mmol) produced a yellow precipitate that was filtered and recrystallized from 1:1 (v/v) CH$_2$Cl$_2$/diethyl ether, collected by filtration, washed with ether, and dried in vacuo. Yield 76%. Anal. Calcd (Found) (%) for C$_{28}$H$_{36}$N$_6$-ClMn$_2$O$_2$PF$_6$: C, 43.18 (43.24); H, 4.66 (4.60); N, 10.79 (10.61). ESI-MS: *m/z* 633 (M$^+$). Selected IR data (cm^{-1}): 3400(br), 2919(m), 1643(s), 1548(s), 1458(m), 1403(s), 1336(m), 1257(w), 1236(s), 1068-(m), 840(br), 557(s).

[Mn$_2$(L)(mcb)](PF$_6$) (1). A solution of mcbNa (0.364 g, 1.54 mmol) in MeOH was added slowly to a solution of [Mn$_2$LCl](PF$_6$) (0.800 g, 1.03 mmol) in CH$_3$CN. The mixture was stirred overnight under N$_2$; the solvent was then evaporated to dryness. The residue was redissolved in CH$_2$Cl$_2$, filtered, and recrystallized twice from 1:1 CH$_2$Cl$_2$/diethyl ether. Yield 70%. Anal. Calcd (Found) (%) for C$_{40}$H$_{45}$N$_8$Mn$_2$O$_4$PF$_6$·CH$_2$-Cl$_2$: C, 47.88 (47.87); H, 4.50 (4.72); N, 10.63 (10.81). ESI-MS: *m/z* 811 (M$^+$). Selected IR data (cm^{-1}): 3434(br), 2920(m), 1644(s), 1552-(s), 1448(s), 1404(s), 1339(s), 1266(w), 1235(s), 1037(m), 840(br), 557-(s). Single crystals suitable for X-ray crystallography were obtained by slow diffusion of diethyl ether into a solution of the compound in CH$_2$Cl$_2$.

[Zn$_2$(L)(mcb)](PF$_6$) (2). Complex **2** was synthesized analogous to complex **1** using ZnCl$_2$ in ethanol.

[Zn$_2$(L)Cl](PF$_6$). Yield 63%. Anal. Calcd (Found) (%) for C$_{28}$H$_{36}$N$_6$-ClO$_2$Zn$_2$PF$_6$·1.7H$_2$O: C, 40.50 (40.49); H, 4.78 (4.58); N, 10.11 (9.88). ESI-MS: *m/z* 655 (M$^+$). Selected IR data (cm^{-1}): 3400(br), 2924(m), 1645(s), 1548(s), 1450(m), 1403(s), 1345(m), 1258(w), 1234(s), 1073-(m), 840(br), 557(s). ^{1}H NMR (CD$_2$Cl$_2$): δ 8.33 (s, 4H, CH=N); 7.18 (s, 4H, Ar); 3.98 (m, 4H, CH$_2$); 3.50 (m, 4H, CH$_2$); 3.01 (m, 8H, CH$_2$); 2.59 (s, 6H, N−CH$_3$); 2.24 (s, 6H, Ar−CH$_3$); 1.56 (s, br, H$_2$O).

[Zn$_2$(L)(mcb)](PF$_6$) (2). Yield 70%. Anal. Calcd (Found) (%) for C$_{40}$H$_{45}$N$_8$Cl$_2$O$_4$Zn$_2$PF$_6$·1.2CH$_2$Cl$_2$: C, 46.56 (46.49); H, 4.37 (4.46); N, 10.24 (10.42). ESI-MS: *m/z* 833 (M$^+$). Selected IR data (cm^{-1}): 3400(br), 2920(m), 1646(s), 1552(s), 1448(s), 1404(s), 1343(s), 1260-(w), 1236(s), 1055(m), 840(br), 557(s). ^{1}H NMR (CD$_2$Cl$_2$): δ 9.06 (s, 1H, (bpy-H^3)); 8.74 (d, 1H, (bpy-H^6)); 8.50 (d, 1H, (bpy-H$^{6'}$)); 8.32 (s, 4H, CH=N); 8.27 (s, 1H, (bpy-H$^{3'}$)); 7.79 (d, 1H, (bpy-H^5)); 7.22 (s, 4H, Ar); 3.76 (m, 4H, CH$_2$); 3.62 (m, 4H, CH$_2$); 2.98 (m, 8H, CH$_2$); 2.71 (s, 6H, N−CH$_3$); 2.44 (s, 3H, (bpy-CH$_3$)); 2.27 (s, 6H, Ar−CH$_3$). Single crystals suitable for X-ray crystallography were obtained from a 1:1:2 CH$_2$Cl$_2$/CH$_3$CN/diethyl ether solution.

4′-Methyl-4-ethylcarboxy-2,2′-bipyridine (mcbEt). 4-Methyl-4′-ethylcarboxy-2,2′-bipyridine (mcbEt) was prepared by a modified literature method.[18] Freshly distilled SOCl$_2$ (7 mL) was added slowly to a suspension of 4′-methyl-2,2′-bipyridine-4-carboxylic acid (1.00 g, 4.67 mmol) in ethanol under a N$_2$ atmosphere. The solution was refluxed for 48 h and evaporated to near dryness (∼95%) under vacuum. The remaining solution was neutralized using an aqueous solution of NaHCO$_3$ and extracted with CH$_2$Cl$_2$ (5 × 50 mL). The organic phase was dried with Na$_2$SO$_4$ and evaporated under a flow of N$_2$. The residue was recrystallized using pentanes (mp 40−42°).[23] Yield 90%. Anal. Calcd (Found) (%) for C$_{14}$H$_{14}$N$_2$O$_2$·0.4C$_2$H$_6$O·0.2H$_2$O: C, 67.26 (67.34); H, 6.41 (6.04); N, 10.60 (10.26). ^{1}H NMR (CD$_2$Cl$_2$): δ 8.90 (dd, *J* = 1.8 Hz, *J* = 0.9 Hz, 1H, 3); 8.78 (dd, *J* = 5.0 Hz, *J* = 0.9 Hz,

(16) Peek, B. M.; Ross, G. T.; Edwards, S. W.; Meyer, G. J.; Meyer, T. J.; Erickson, B. W. *Int. J. Pept. Protein Res.* **1991**, *38*, 114−123.
(17) Wehman, P.; Dol, G. C.; Moorman, E. R.; Kramer, P. C. J.; van Leeuwen, P. W. N. M.; Fraanje, J.; Goubitz, K. *Organometallics* **1994**, *13*, 4856−4869.
(18) Sprintschnik, G.; Sprintschnik, H. W.; Kirsch, P. P.; Whitten, D. G. *J. Am. Chem. Soc.* **1977**, *99*, 4947−4954.
(19) Huang, W. S. G.; Hu, D.; Meng, Q. *Synth. Commun.* **2000**, *30* (9), 1555−1561.
(20) Damrauer, N. H.; Boussie, T. R.; Devenney, M.; McCusker, J. K. *J. Am. Chem. Soc.* **1997**, *119*, 8253−8268.
(21) Anderson, P. A.; Anderson, R. F.; Furue, M.; Junk, P. C.; Keene, F. R.; Patterson, B. T.; Yeomans, B. D. *Inorg. Chem.* **2000**, *39*, 2721−2728.

(22) Nagata, T.; Ikawa, Y.; Maruyama, K. *Chem. Commun.* **1994**, 471−472.
(23) Launikonis, A.; Lay, P. A.; Mau, A. W.-H.; Sargeson, A. M.; Sasse, W. H. F. *Aust. J. Chem.* **1986**, *39*, 1053−1062.

1H, 6); 8.55 (d, $J = 5$ Hz, 1H, 6′); 8.29 (s, 1H, 3′); 7.85 (dd, $J = 5$ Hz, $J = 1.8$ Hz, 1H, 5); 7.18 (d, $J = 5$ Hz, 1H, 5′); 4.44 (q, $J = 7$ Hz, 2H, Et−CH$_2$); 2.45 (s, 3H, 4′-CH$_3$); 1.43 (t, $J = 7$ Hz, 3H, Et−CH$_3$).

[Ru((CH$_3$)$_2$-bpy)$_2$(mcbEt)](PF$_6$)$_2$. This compound was synthesized following a modified literature procedure from Ru((CH$_3$)$_2$-bpy)$_2$Cl$_2$ and mcbEt.[24] The product was recrystallized by ether diffusion into a CH$_2$Cl$_2$ solution. Yield 68%. Anal. Calcd (Found) (%) for C$_{38}$H$_{38}$N$_6$O$_2$-RuF$_{12}$P$_2$·0.4CH$_2$Cl$_2$: C, 44.60 (44.68); H, 3.74 (3.99); N, 8.00 (8.02). ESI-MS: m/z 356 (M^{2+}), 857 ((M−PF$_6$)$^+$).

[Ru((CF$_3$)$_2$-bpy)$_2$(mcbEt)](PF$_6$)$_2$. This compound was synthesized following a modified literature procedure from Ru((CH$_3$)$_2$-bpy)$_2$Cl$_2$ and mcbEt.[24] The product was recrystallized from a 1:1:2 acetone/CH$_2$Cl$_2$/ether mixture. Yield 58%. Anal. Calcd (Found) (%) for C$_{38}$H$_{26}$N$_6$O$_2$-RuF$_{24}$P$_2$·1.5CH$_2$Cl$_2$: C, 36.13 (36.05); H, 2.14 (2.32); N, 6.16 (6.34). MS: m/z 464 (M^{2+}), 1073 ((M−PF$_6$)$^+$).

[Mn$_2$(L)(mcb)(Ru((CH$_3$)$_2$-bpy)$_2$)](PF$_6$)$_3$ (3). Under a N$_2$ atmosphere, Ru((CH$_3$)$_2$-bpy)$_2$Cl$_2$ (0.190 g, 0.352 mmol) and thallium hexafluorophosphate (0.252 g, 0.721 mmol) were combined in acetone and stirred at room temperature in the dark. The reaction was monitored by UV−vis spectroscopy during which time a shift of the absorption feature at 560 to 500 nm signaled the formation of the [Ru((CH$_3$)$_2$-bpy)$_2$-(acetone)$_2$]$^{2+}$ product. Once the absorption spectrum stopped changing, the solution was filtered through Celite, and the solvent was removed by vacuum distillation to dryness. The resulting residue was dissolved in CH$_2$Cl$_2$, filtered again through Celite, and then slowly added to a dichloromethane solution of complex **1** (0.404 g, 0.422 mmol) under N$_2$ in the dark. The reaction was monitored by UV−vis spectroscopy over a period of several days during which time a decrease in intensity of the band at 500 nm concomitant with the formation of a new Ru-based charge-transfer feature at 470 nm indicated the formation of the desired compound. The product was isolated by precipitation following addition of diethyl ether and then recrystallized several times from a mixture of 1:1 CH$_2$Cl$_2$/Et$_2$O to yield an analytically pure product. Yield 30%. Anal. Calcd. (Found) (%) for C$_{64}$H$_{69}$Mn$_2$N$_{12}$O$_4$RuP$_3$F$_{18}$·0.7CH$_2$Cl$_2$: C, 44.03 (44.06); H, 3.98 (4.18); N, 9.42 (9.27). ESI-MS: m/z 427 (M^{3+}).

[Mn$_2$(L)(mcb)(Ru((CF$_3$)$_2$-bpy)$_2$)](PF$_6$)$_3$ (4). This compound was prepared analogously to compound **3** with the exception that AgPF$_6$ was used in the place of TlPF$_6$. A shift in the absorption spectrum from 580 to 500 nm was monitored to signal formation of [Ru((CF$_3$)$_2$-bpy)$_2$(acetone)$_2$]$^{2+}$, and subsequent disappearance of the 500 nm band in the reaction with complex **1** indicated the formation of the desired compound. Yield 37%. Anal. Calcd. (Found) (%) for C$_{64}$H$_{57}$N$_{12}$Mn$_2$O$_4$-RuP$_3$F$_{30}$·0.4(C$_2$H$_5$)$_2$O: C, 40.17 (40.20); H, 3.13 (3.04); N, 8.57 (8.60). ESI-MS: m/z 499 (M^{3+}), 821 ((M−PF$_6$)$^{2+}$), 1787 ((M−2PF$_6$)$^+$).

[Zn$_2$(L)(mcb)(Ru((CH$_3$)$_2$-bpy)$_2$)](PF$_6$)$_3$ (5). This complex was prepared analogously to complex **3** by replacing [Mn$_2$(L)(mcb)](PF$_6$) (**1**) with [Zn$_2$(L)(mcb)](PF$_6$) (**2**). Yield 35%. Anal. Calcd. (Found) (%) for C$_{64}$H$_{69}$N$_{12}$O$_4$RuZn$_2$P$_3$F$_{18}$·(C$_2$H$_5$)$_2$O: C, 45.10 (45.06); H, 4.40 (4.57); N, 9.28 (9.30). ESI-MS: m/z 434 (M^{3+}), 723 ((M−PF$_6$)$^{2+}$).

[Zn$_2$(L)(mcb)(Ru((CF$_3$)$_2$-bpy)$_2$)](PF$_6$)$_3$ (6). This compound was prepared analogously to complex **4** by replacing [Mn$_2$(L)(mcb)](PF$_6$) (**1**) with [Zn$_2$(L)(mcb)](PF$_6$) (**2**). Yield 30%. Anal. Calcd. (Found) (%) for C$_{64}$H$_{57}$N$_{12}$O$_4$RuZn$_2$P$_3$F$_{30}$·(C$_2$H$_5$)$_2$O: C, 40.29 (40.48); H, 3.33 (3.37); N, 8.29 (8.57). ESI-MS: m/z 506 (M^{3+}), 831 (M−PF$_6$)$^{2+}$).

Physical Measurements: Electrochemistry. Cyclic and differential pulse voltammetry measurements were carried out in a N$_2$-filled drybox (Vacuum Atmospheres) using a BAS CV-50W electrochemical analyzer. Compounds were dissolved in CH$_2$Cl$_2$ that had been distilled over CaH$_2$ and thoroughly degassed; NBu$_4$PF$_6$ (0.1 M) was added as the supporting electrolyte. A standard three-electrode setup was employed consisting of Pt working and counter electrodes and Ag/AgNO$_3$ (1 mM of AgNO$_3$ in CH$_3$CN) as the reference electrode. Potentials are given versus the ferrocene/ferrocenium couple, which

---

(24) Mabrouk, P. A.; Wrighton, M. S. *Inorg. Chem.* **1986**, *25*, 526−531.

Table 1. Crystallographic Data for [Mn$_2$(L)(mcb)](PF$_6$)·CH$_2$Cl$_2$ (**1**) and [Zn$_2$(L)(mcb)](PF$_6$)·CH$_3$CN (**2**)

	1	2
mol formula	C$_{41}$H$_{47}$Cl$_2$F$_6$Mn$_2$N$_8$O$_4$P	C$_{42}$H$_{48}$F$_6$N$_9$O$_4$PZn$_2$
fw (g/mol)	1041.62	1018.60
cryst color, habit	yellow, blocks	brown, blocks
cryst system	monoclinic	monoclinic
space group	$P2(1)/c$	$P2(1)/c$
temp (K)	173(2)	173(2)
cell dimensions		
a (Å)	13.654(3)	13.257(2)
b (Å)	22.228(4)	22.498(3)
c (Å)	15.352(3)	14.956(2)
α (°)	90.00	90.00
β (°)	103.990(3)	99.742(2)
γ (°)	90.00	90.00
V (Å^3)	4521.2(14)	4396.4(9)
Z	4	4
ρ_{calcd} (g cm^{-3})	1.530	1.539
GOF (F^2)	1.034	0.984
$R_1{}^a$	0.0713	0.0390
w$R_2{}^b$	0.1464	0.0671

^{a} $R_1 = \Sigma||F_o| - |F_c||/\Sigma|F_o|$. ^{b} $wR_2 = [\Sigma w(F_o{}^2 - F_c{}^2)^2/\Sigma w(F_o{}^2)^2]^{1/2}$, $w = 1/[\sigma^2(F_o{}^2) + (aP)^2 + bP]$, where $P = [F_o{}^2 + 2F_c{}^2]/3$.

was used as an internal standard, and are quoted as $E_{1/2}$ values according to the DPV peaks.[25] Low-temperature measurements were achieved by immersing the cell in a dry ice/acetone bath; the Ag/AgNO$_3$ reference was kept (nominally) at room temperature but in contact with the low-temperature solution using a salt bridge. Data acquired for the ferrocene/ferrocenium couple using this setup did not reveal any systematic variations in redox potential as the temperature was varied between −65 °C and room temperature.

X-ray Structure Determination. Single-crystal X-ray diffraction data for complexes **1** and **2** were acquired at the X-ray facility of Michigan State University. Diffraction data were collected on a Siemens SMART diffractometer with graphite-monochromatic Mo Kα radiation ($\lambda = 0.71073$ Å). Data were collected at −100 °C by using an Oxford Cryosystems low-temperature device. Crystallographic data are summarized in Table 1. Lattice parameters were obtained from least-squares analyses. Data were integrated with the program SAINT.[26] The integration method employed a three-dimensional profiling algorithm; all data were corrected for Lorentz and polarization factors as well as for crystal decay effects. The absorption correction program SADABS[27] was employed to correct the data for absorption effects. The structures were solved by direct methods and expanded using Fourier techniques. All structure calculations were performed with the SHELXTL 6.12 software package.[28] Anisotropic thermal parameters were refined for all non-hydrogen atoms. Hydrogen atoms were localized in their calculation positions and refined by using the riding model. Further details concerning the structure determinations may be found in the Supporting Information.

Steady-State and Time-Resolved Spectroscopies. All spectroscopic data were obtained on samples prepared in an Ar atmosphere drybox in sealed quartz cuvettes. Samples were dissolved in dichloromethane that had been distilled from CaH$_2$, degassed, and stored under an argon atmosphere. For steady-state and nanosecond time-resolved emission measurements, samples were placed in 10 mm path length cells. Ground-state absorption spectra were recorded using a Hewlett-Packard 8452A diode array spectrophotometer. Steady-state emission spectra were acquired using a Spex FluoroMax fluorimeter. Emission spectra were corrected for instrumental response by using a NIST standard of spectral irradiance (Optronic Laboratories, Inc., OL220M tungsten

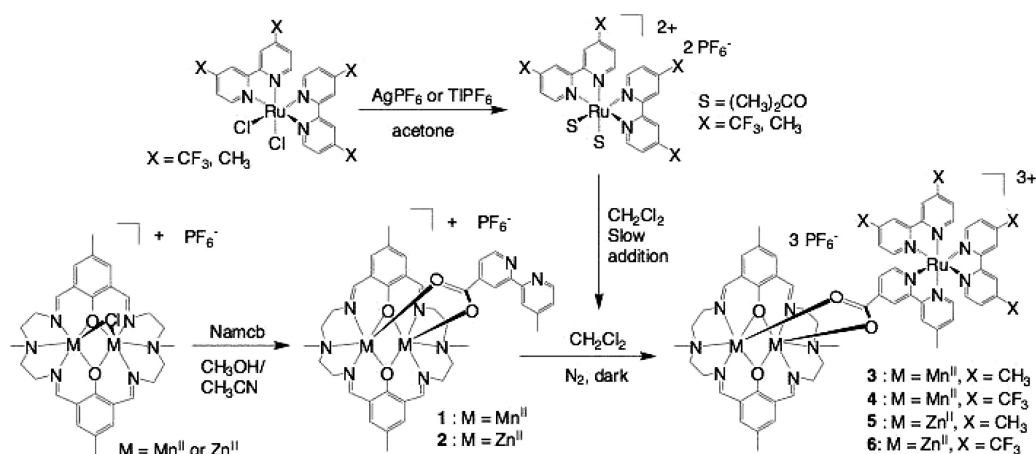(25) Richardson, D. E.; Taube, H. *Inorg. Chem.* **1981**, *20*, 1278−1285.
(26) *SAINT, ver. 6.02a*; Bruker AXS, Inc.: Madison, WI, 2000.
(27) Sheldrick, G. M. *SADABS, ver. 2.03*; Bruker AXS, Inc.: Madison, WI, 2000.
(28) Sheldrick, G. M. *SHELXTL, ver. 6.12*; Bruker AXS, Inc.: Madison, WI, 2001.

Scheme 2

quartz lamp). All subsequent data manipulations were carried out with the corrected spectra as described elsewhere.[20]

Relative radiative quantum yields (Φ_r) were determined on optically thin solutions (o.d. ~0.1) using [Ru(bpy)$_3$](PF$_6$)$_2$ as a standard (Φ_r = 0.029 in dichloromethane[29]). Quantum yields were calculated according to eq 1

$$\Phi_{unk} = \Phi_{std} \frac{(I_{unk}/A_{unk})}{(I_{std}/A_{std})} \left(\frac{\eta_{unk}}{\eta_{std}}\right)^2 \qquad (1)$$

where Φ_{unk} and Φ_{std} are the radiative quantum yields of the sample and standard, I_{unk} and I_{std} are the integrated emission intensities of the corrected spectra for the sample and standard, A_{unk} and A_{std} are the absorbances of the sample and standard at the excitation wavelength (470 nm in all cases), and η_{unk} and η_{std} are the indices of refraction of the sample and standard solutions (taken to be equivalent to the neat solvent), respectively.

Nanosecond time-resolved absorption measurements were carried out using a Nd:YAG-based laser spectrometer that has been described previously.[20] Excitation energies at the sample were in the range of 1−3 mJ/pulse; all data were checked for linearity with respect to pump power. The apparatus used for acquisition of emission data via picosecond time-correlated single photon counting (TCSPC) is described elsewhere.[30] The absorbance of each sample at the excitation wavelength (470 nm) was in the range of 0.1−0.15 for the steady-state and time-resolved emission measurements and 0.5−0.9 for time-resolved absorption measurements. The absorption spectrum of each sample was measured before and after all photophysical measurements to verify the integrity of the sample.

Ultrafast measurements were carried out as described elsewhere.[31] Typical pump powers were 6−7 μJ for excitation at 470 nm. Samples were dissolved in distilled CH$_2$Cl$_2$ in an Ar atmosphere drybox and placed in 1 mm path length quartz cuvettes. Typical absorbance values were ~0.7 at the excitation wavelength. The data were checked for linearity with respect to pump power to ensure that the observed kinetics were due to single-photon excitation. All data manipulations (e.g., integrated emission intensities, fits to appropriate kinetic models, etc.) were carried out using the Origin software package, SigmaPlot, or the IgorPro data analysis suite by WaveMetrics, Inc.

Variable-Temperature Measurements. Steady-state and nanosecond time-resolved spectroscopies were performed using a Janis SVT-100 optical cryostat. Samples were thoroughly degassed, sealed in a cylindrical sample holder, and placed within the dewar. Temperature control was achieved using two Lake Shore model 321-01 temperature

controllers with two matched diodes placed approximately equidistant above and below the sample region. Temperature stability using this configuration was better than ±0.5 K; the absolute accuracy is estimated to be ±1 K. The samples were allowed to equilibrate for 10 min at each temperature prior to data collection. Measurements were carried out in freshly distilled CH$_2$Cl$_2$ for fluid solution studies and a mixture of CH$_2$Cl$_2$/2-MeTHF (~2:1) for measurements in low-temperature optical glasses. Electrochemical measurements at room temperature did not reveal any significant differences in the redox behavior of compounds between these two solvent systems. Furthermore, variable-temperature spectroscopic data acquired above the glass-to-fluid transition temperature of the CH$_2$Cl$_2$/2-MeTHF mixture yielded rate constants that were within experimental error of data acquired in neat CH$_2$Cl$_2$. Fitting of the steady-state emission spectra to eq 6 (vide infra) was performed using a program developed by Dr. Juan-Pablo Claude.[32]

Results and Discussion

Syntheses. The synthetic procedure for the preparation of complexes **1**−**6** is summarized in Scheme 2. The target assemblies—[Mn$_2$(L)(mcb)(Ru(X$_2$-bpy)$_2$)](PF$_6$)$_3$ (X = CH$_3$ (**3**) or CF$_3$ (**4**))—are the product of the reaction of an in situ-generated [Ru(X$_2$-bpy)$_2$(acetone)$_2$]$^{2+}$ complex with an excess of [Mn$_2$(L)(mcb)](PF$_6$) (**1**), where the 4-methyl-4′-carboxy-2,2′-bipyridine (mcb) ligand connects the dimanganese(II) core to the Ru^{II} polypyridyl center. Synthesis of the Zn^{II}-containing model complexes, [Zn$_2$(L)(mcb)(Ru(X$_2$-bpy)$_2$)](PF$_6$)$_3$ (X = CH$_3$ (**5**) or CF$_3$ (**6**)), follows the same strategy by reacting the ruthenium complex with [Zn$_2$(L)(mcb)](PF$_6$) (**2**).

Complexes of the form [M$_2$(L)(mcb)](PF$_6$) (where M = Mn^{II} and Zn^{II} for **1** and **2**, respectively) were each synthesized in two-step reactions. First, the chloro-bridged precursor [M$_2$(L)-Cl](PF$_6$) was obtained by template condensation of *N,N*-bis(2-aminoethyl)-*N*-methylamine and 2,6-diformyl-4-methylphenol in the presence of the appropriate metal chloride salt. The reaction was performed under N$_2$ to prevent the oxidation of Mn^{II} (complex **1**) or in the case of complex **2** to maintain an anhydrous environment. Once these intermediate compounds were isolated and characterized, addition of sodium 4′-methyl-2,2′-bipyridine-4-carboxylate (mcbNa) in methanol to a solution of either [Mn$_2$(L)Cl](PF$_6$) or [Zn$_2$(L)Cl](PF$_6$) in acetonitrile, followed by stirring at room temperature for several hours, yielded the desired products.

Single crystals of complexes **1** and **2** suitable for X-ray diffraction studies were obtained from slow diffusion of diethyl

(29) Caspar, J. V.; Meyer, T. J. *J. Am. Chem. Soc.* **1983**, *105*, 5583−5590.
(30) DeWitt, L.; Blanchard, G. J.; LeGoff, E.; Benz, M. E.; Liao, J. H.; Kanatzidis, M. G. *J. Am. Chem. Soc.* **1993**, *115*, 12158−12164.
(31) Juban, E. A.; McCusker, J. K. *J. Am. Chem. Soc.* **2005**, *127*, 6857−6865.

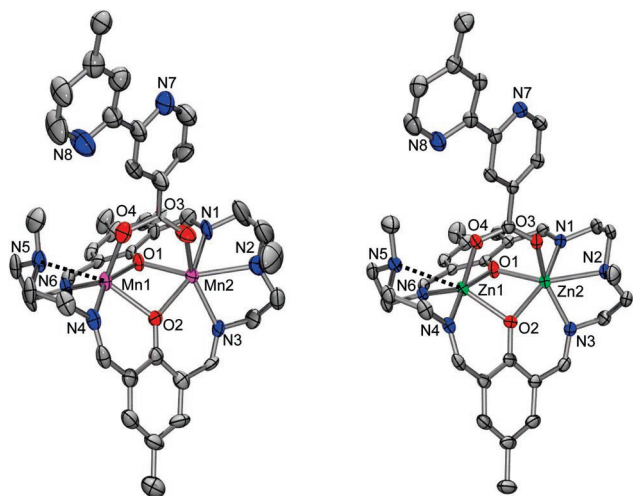(32) Claude, J. P.; Meyer, T. J. *J. Phys. Chem.* **1995**, *99*, 51−54.

Figure 1. Drawings of the cations of [Mn₂(L)(mcb)](PF₆)·CH₂Cl₂ (**1**, left) and [Zn₂(L)(mcb)](PF₆)·CH₃CN (**2**, right) obtained from single-crystal X-ray structure determinations. Atoms are shown as 50% thermal ellipsoid representations. The hydrogen atoms, PF₆⁻ counterion, and solvate molecules have been omitted for clarity. Dashed lines show the long bond distances described in the text.

ether into dichloromethane for complex **1** and from a mixture of dichloromethane, acetonitrile, and diethyl ether for complex **2**. Drawings of these two structures are shown in Figure 1; selected bond distances and angles are given in Table 2. [Mn₂-(L)(mcb)](PF₆)·CH₂Cl₂ (**1**) crystallizes in the monoclinic space group $P2(1)/c$ with the [Mn₂(L)(mcb)]⁺ cation located on a general position. In addition to the [Mn₂(L)(mcb)]⁺ cation, the asymmetric unit contains one hexafluorophosphate anion and one molecule of CH₂Cl₂. The cation consists of a Schiff-base macrocycle ligand (L) and two Mn²⁺ ions bridged by the two phenolic oxygens from the Schiff-base macrocycle and the carboxylate of a mcb ligand. The remainder of the Mn ion coordination spheres derives from the two imine nitrogen atoms and a secondary aliphatic nitrogen atom from the macrocycle. In the case of the manganese–secondary amine interaction, the Mn1–N5 distance is much longer than the analogous bond to Mn2 (2.613 Å vs 2.438 Å), resulting in a degree of asymmetry between the two Mn sites. Nevertheless, all of the bond distances fall in the range typically observed for similar Mnᴵᴵ-Schiff-base complexes.[33,34] The longer Mn1–N5 distance is indicated with a dashed line in Figure 1.

[Zn₂(L)(mcb)](PF₆)·CH₃CN (**2**) also crystallizes in the monoclinic space group $P2(1)/c$. The asymmetric unit contains the [Zn₂(L)(mcb)]⁺ cation, one hexafluorophosphate anion, and one molecule of CH₃CN. The cation is composed of a Schiff-base macrocycle ligand, two Zn²⁺ ions, and the mcb ligand; many of the structural features of complex **2** are similar to a related macrocyclic system reported by Dutta et al.[35] Inspection of both Figure 1 and Table 2 reveals that complexes **1** and **2** are essentially isostructural save for minor differences due to the smaller ionic radius of Zn²⁺ relative to Mn²⁺. Of particular note is the elongated metal–amine bond in this compound (Zn1–N5), resulting in a similar degree of asymmetry within the dinuclear metal core as found for complex **1**. The metal–metal distances in the two complexes are slightly different (3.280 Å

(33) Nagata, T.; Mizukami, J. *J. Chem. Soc., Dalton Trans.* **1995**, 2825–2830.
(34) Ikawa, Y.; Nagata, T.; Maruyama, K. *Chem. Lett.* **1993**, 1049–1052.
(35) Dutta, B.; Bag, P.; Florke, U.; Nag, K. *Inorg. Chem.* **2005**, *44*, 147–157.

Table 2. Selected Bond-Distances (Å) and Angles (deg) for [Mn₂(L)(mcb)](PF₆)·CH₂Cl₂ (**1**) and [Zn₂(L)(mcb)](PF₆)·CH₃CN (**2**)

	1		**2**
		Bond Distances (Å)	
Mn(1)−N(4)	2.186(8)	Zn(1)−N(4)	2.091(2)
Mn(1)−N(6)	2.183(8)	Zn(1)−N(6)	2.072(2)
Mn(1)−O(1)	2.212(6)	Zn(1)−O(1)	2.164(2)
Mn(1)−O(2)	2.204(6)	Zn(1)−O(2)	2.110(2)
Mn(1)−O(4)	2.086(7)	Zn(1)−O(4)	1.993(2)
Mn(2)−N(1)	2.232(8)	Zn(2)−N(1)	2.131(2)
Mn(2)−N(2)	2.438(9)	Zn(2)−N(2)	2.317(2)
Mn(2)−N(3)	2.193(8)	Zn(2)−N(3)	2.086(2)
Mn(2)−O(1)	2.195(6)	Zn(2)−O(1)	2.102(2)
Mn(2)−O(2)	2.178(6)	Zn(2)−O(2)	2.123(2)
Mn(2)−O(3)	2.132(7)	Zn(2)−O(3)	2.065(2)
Mn(1)···Mn(2)ᵃ	3.280	Zn(1)···Zn(2)ᵃ	3.215
Mn(1)···N(5)ᵇ	2.618	Zn(1)···N(5)ᵇ	2.813
		Bond Angles (deg)	
Mn(2)−O(1)−Mn(1)	96.2(2)	Zn(2)−O(1)−Zn(1)	97.81(6)
Mn(2)−O(2)−Mn(1)	96.9(2)	Zn(1)−O(2)−Zn(2)	98.86(6)
O(2)−Mn(1)−O(1)	74.7(2)	O(2)−Zn(1)−O(1)	73.59(6)
O(4)−Mn(1)−O(1)	90.9(2)	O(4)−Zn(1)−O(1)	91.36(6)
O(4)−Mn(1)−O(2)	100.7(2)	O(4)−Zn(1)−O(2)	103.31(6)
N(4)−Mn(1)−O(1)	153.4(3)	N(4)−Zn(1)−O(1)	155.93(7)
N(6)−Mn(1)−O(1)	80.7(3)	N(6)−Zn(1)−O(1)	83.93(7)
N(4)−Mn(1)−O(2)	78.8(3)	N(4)−Zn(1)−O(2)	82.56(7)
N(6)−Mn(1)−O(2)	119.6(3)	N(6)−Zn(1)−O(2)	123.82(7)
O(4)−Mn(1)−N(4)	94.7(3)	O(4)−Zn(1)−N(4)	97.37(7)
O(4)−Mn(1)−N(6)	134.2(3)	O(4)−Zn(1)−N(6)	128.50(7)
N(6)−Mn(1)−N(4)	112.6(3)	N(6)−Zn(1)−N(4)	107.36(7)
O(1)−Mn(2)−O(2)	75.5(2)	O(1)−Zn(2)−O(2)	74.58(6)
O(3)−Mn(2)−O(2)	93.4(2)	O(3)−Zn(2)−O(2)	91.36(6)
O(3)−Mn(2)−O(1)	92.4(3)	O(3)−Zn(2)−O(1)	88.58(6)
O(1)−Mn(2)−N(1)	80.1(3)	O(1)−Zn(2)−N(1)	83.69(7)
O(1)−Mn(2)−N(2)	153.8(3)	O(1)−Zn(2)−N(2)	158.89(7)
O(1)−Mn(2)−N(3)	117.8(3)	O(1)−Zn(2)−N(3)	117.68(7)
O(2)−Mn(2)−N(1)	155.2(3)	O(2)−Zn(2)−N(1)	157.17(7)
O(2)−Mn(2)−N(2)	130.7(3)	O(2)−Zn(2)−N(2)	124.59(7)
O(2)−Mn(2)−N(3)	80.4(3)	O(2)−Zn(2)−N(3)	83.99(7)
O(3)−Mn(2)−N(1)	91.8(3)	O(3)−Zn(2)−N(1)	95.07(7)
O(3)−Mn(2)−N(2)	86.2(3)	O(3)−Zn(2)−N(2)	82.65(6)
O(3)−Mn(2)−N(3)	145.9(3)	O(3)−Zn(2)−N(3)	150.65(7)
N(1)−Mn(2)−N(2)	73.8(3)	N(1)−Zn(2)−N(2)	78.04(7)
N(3)−Mn(2)−N(2)	73.4(3)	N(3)−Zn(2)−N(2)	76.42(7)
N(3)−Mn(2)−N(1)	107.8(3)	N(3)−Zn(2)−N(1)	100.38(8)

ᵃ Nonbonding metal-to-metal distance. ᵇ This distance was measured from the crystal structure but is not contained in the cif file.

vs 3.215 Å for **1** and **2**, respectively) but still similar enough to avoid significant differences in the metrics associated with the bridging mcb group. We have been unsuccessful in our efforts to obtain X-ray quality crystals of the ruthenium polypyridyl adducts of complexes **1** and **2**. Nevertheless, the isostructural nature of two compounds just described gives us confidence that the Znᴵᴵ₂ analogs will serve as excellent models for interpreting the properties of complexes **3** and **4**.

Once complexes [Mn₂(L)(mcb)](PF₆) (**1**) and [Zn₂(L)(mcb)]-(PF₆) (**2**) were available, the next step was to bind them to the different Ru moieties. For this purpose, two intermediate *cis*-[Ru(X₂-bpy)₂(acetone)₂](PF₆)₂ (X = CH₃, CF₃) complexes were synthesized from Ru(X₂-bpy)₂Cl₂. As will be elaborated upon later, these two adducts were chosen because of the different electron-donating ability of the groups in the 4 and 4′ positions of the bipyridine ligands. The more substitutionally labile solvento species were synthesized by addition of TlPF₆ (X = CH₃) or AgPF₆ (X = CF₃) to dry acetone solutions of Ru(X₂-bpy)₂Cl₂; TlPF₆ was used in the case of Ru(CH₃-bpy)₂Cl₂ due to the fact that this compound was found to be susceptible to oxidation in the presence of Ag⁺. The progress of this reaction

is most easily monitored by UV−vis spectroscopy due to the change in absorption that occurs upon replacing Cl⁻ for acetone. This reaction was carried out under an N_2 atmosphere in the absence of light so as to prevent side reactions such as ligand exchange, oxidation, and/or dimerization of the ruthenium species as seen previously.[36] After filtration to remove the metal-chloride side product, the acetone solution was evaporated to dryness, and the intermediate product, $[Ru(X_2\text{-bpy})_2(\text{acetone})_2]$-$(PF_6)_2$, was redissolved. Slow addition of a CH_2Cl_2 solution of this solvento species to CH_2Cl_2 solutions of either $[Mn_2(L)$-$(mcb)](PF_6)$ (**1**) or $[Zn_2(L)(mcb)](PF_6)$ (**2**) yielded the corresponding Ru polypyridyl adducts, complexes **3**−**6**. These reactions took several days of stirring at room temperature to complete; heating the reaction turned out to be counterproductive due to the formation of side products and labilization of the mcb ligand. Running the reaction with a slight excess of the Mn_2 (or Zn_2) starting material generally resulted in higher yields. This reaction was again monitored via electronic absorption spectroscopy, specifically by tracking the change in the MLCT absorption profile of the chromophore upon binding to the mcb ligand. Once the reaction was complete (i.e., once the UV−vis spectrum stopped changing), addition of diethyl ether resulted in the precipitation of the final product from the reaction mixture. This material had to be recrystallized multiple times from dichloromethane/ether mixtures in order to obtain a pure product.

Absent an X-ray structure, characterization of the final products, $[Mn_2(L)(mcb)(Ru(X_2\text{-bpy})_2)](PF_6)_3$ (X = CH_3 (**3**), CF_3 (**4**)) and $[Zn_2(L)(mcb)(Ru(X_2\text{-bpy})_2)](PF_6)_3$ (X = CH_3 (**5**), CF_3 (**6**)), was achieved primarily through elemental analysis and mass spectroscopy. The latter technique was particularly informative. Figure S1 shows the ESI-MS spectra for complexes **3**−**6** obtained from CH_2Cl_2 solutions. The excellent agreement between the experimental and calculated isotope patterns provides compelling evidence of the identity of complexes **3**−**6** and, more importantly, that they remain intact in solution.

Physical Characterization. Electronic Absorption Spectroscopy. The ground-state electronic absorption spectra of complexes **1**−**6** have been measured in CH_2Cl_2. Two main features are observed in the blue and near-UV regions in both $[Mn_2(L)(mcb)](PF_6)$ (**1**) and $[Zn_2(L)(mcb)](PF_6)$ (**2**) (Figure S2). Given their striking similarity in terms of both energy and band shape, we can immediately ascribe both bands in the two complexes as being endemic to the Schiff-base macrocycle ligand. The lowest energy absorption near 390 nm is assigned to a $\pi \rightarrow \pi^*$ transition involving the azomethene group;[37] this feature shifts slightly from 385 to 390 nm upon binding to Zn^{II} versus Mn^{II}. There is also a weak shoulder observed at ~300 nm, identified for both complexes, that is presently unassigned. The strong band around 260 nm has been assigned to a $\pi \rightarrow \pi^*$ transition associated with the phenolic chromophore.[37] Of particular note is the complete absence of any absorptions in the visible region of the spectrum. This is to be expected for both of these compounds given the d^{10} configuration of Zn^{II}
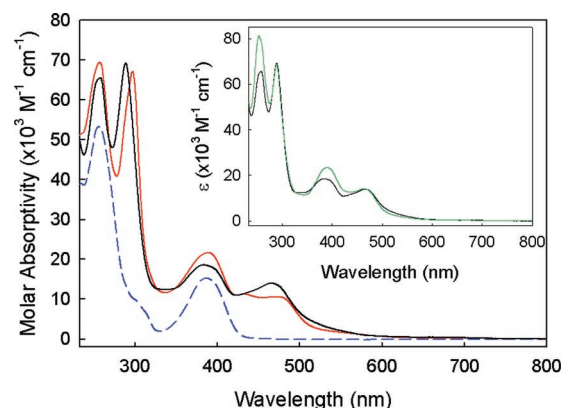

Figure 2. Electronic absorption spectra of $[Mn_2(L)(mcb)(Ru((CH_3)_2\text{-bpy})_2)]$-$(PF_6)_3$ (**3**, black line), $[Mn_2(L)(mcb)(Ru((CF_3)_2\text{-bpy})_2)](PF_6)_3$ (**4**, red line), and $[Mn_2(L)(mcb)](PF_6)$ (**1**, blue dashed line) in CH_2Cl_2 solution at room temperature. The inset shows the electronic absorption spectra of $[Mn_2$-$(L)(mcb)(Ru((CH_3)_2\text{-bpy})_2)](PF_6)_3$ (**3**, black line) and $[Zn_2(L)(mcb)$-$(Ru((CH_3)_2\text{-bpy})_2)](PF_6)_3$ (**5**, green line) for comparison.

and the fact that both Mn^{II} ions in complex **2** are high-spin;[38,39] however, this point will become significant for interpreting the photophysical behavior of the Ru^{II} adducts of these systems.

The electronic absorption spectra of $[Mn_2(L)(mcb)(Ru((CH_3)_2\text{-bpy})_2)](PF_6)_3$ (**3**) and $[Mn_2(L)(mcb)(Ru((CF_3)_2\text{-bpy})_2)]$-$(PF_6)_3$ (**4**) are shown in Figure 2, along with the spectrum of $[Mn_2(L)(mcb)](PF_6)$ (**1**). As mentioned above, the Schiff-base macrocycle ligand exhibits two intraligand transitions at 260 and 390 nm. The principal difference upon introduction of the Ru^{II} polypyridyl fragment is the presence of new absorptions in the 450−500 nm region; these features are characteristic of the $^1A_1 \rightarrow {}^1MLCT$ absorption(s) endemic to this class of compounds. We also observe a strong new absorption band in the ultraviolet for both complexes **3** and **4**, readily assigned as a $\pi \rightarrow \pi^*$ transition(s) of the bipyridyl ligands. Although the spectra for complexes **3** and **4** are similar, differences due to the influence of the 4,4′ substituents on the peripheral bpy ligands are evident. Specifically, we note a red-shift in both the $\pi \rightarrow \pi^*$ absorption (288 nm vs 296 nm) and the MLCT bands (470 nm vs 484 nm) reflecting the more electron-withdrawing nature of the CF_3 group relative to CH_3.[40] The impact of this change can also be seen in the electrochemical properties of the compounds (vide infra), the nature of the lowest-energy excited state, and ultimately the dynamics of this system following photoexcitation. These points not withstanding, the inset in Figure 2 clearly shows that the optical characteristics of the Mn_2^{II} and corresponding Zn_2^{II} analog are virtually identical. This observation underscores the utility of the Zn_2^{II} complexes as excellent models for interpreting photoinduced dynamics due to the presence of the (optically silent) Mn_2^{II} core.

Electrochemistry. The electrochemical properties of $[Mn_2$-$(L)(mcb)](PF_6)$ (**1**) and the two Mn^{II}-containing ruthenium

(36) Weaver, T. R.; Meyer, T. J.; Adeyemi, S. A.; Brown, G. M.; Eckberg, R. P.; Hatfield, W. E.; Johnson, E. C.; Murray, R. W.; Untereker, D. *J. Am. Chem. Soc.* **1975**, *97*, 3039−3048.
(37) Bosnich, B. *J. Am. Chem. Soc.* **1968**, *90*, 627−632.

(38) Magnetic susceptibility measurements indicate weak antiferromagnetic exchange between the two Mn^{II} ions in this class of compounds, giving rise to a room-temperature effective moment of $\mu_{eff} \approx 8 \mu_B$. Further details concerning the magnetic properies of these compounds will be published elsewhere.
(39) Due to the nature of the ground state of six-coordinate high-spin d^5 metal complexes ($^6A_1$), there are no spin-allowed ligand-field bands possible. Spin exchange can alter this situation in principle, but the absence of any features in the absorption spectrum of $[Mn_2(L)(mcb)](PF_6)$ (**1**) indicates that such effects are minor in the present case.
(40) Furue, M.; Maruyama, K.; Oguni, T.; Naiki, M.; Kamachi, M. *Inorg. Chem.* **1992**, *31*, 3792−3795.

Table 3. Electrochemical Data for Complexes **1**, **3**, **4**, and [Ru(X$_2$-bpy)$_2$(mcbEt)](PF$_6$)$_2$ (X = CH$_3$, CF$_3$) in CH$_2$Cl$_2$ Solution[a]

	oxidations			reductions		
complex	Mn$^{II}_2$/Mn^{II}Mn^{III}	Mn^{II}Mn^{III}/Mn$^{III}_2$	Ru^{II}/Ru^{III}	$E_{1/2}^{red1}$	$E_{1/2}^{red2}$	$E_{1/2}^{red3}$
[Mn$_2$(L)(mcb)](PF$_6$) (**1**)	+0.08	+0.43		−2.00		
[Mn$_2$(L)(mcb)(Ru((CH$_3$)$_2$-bpy)$_2$)](PF$_6$)$_3$ (**3**)	+0.23	∼+0.7[b]	∼+0.7[b]	−1.58	−1.95	
[Mn$_2$(L)(mcb)(Ru((CF$_3$)$_2$-bpy)$_2$)](PF$_6$)$_3$ (**4**)	+0.28	+0.63	+1.12	−1.17	−1.40	−1.85
[Ru((CH$_3$)$_2$-bpy)$_2$(mcbEt)](PF$_6$)$_2$			+0.79	−1.52	−2.00	
[Ru((CF$_3$)$_2$-bpy)$_2$(mcbEt)](PF$_6$)$_2$			+1.14	−1.15	−1.38	−1.83

[a] Potentials are reported versus the ferrocene/ferrocenium couple as described in the Experimental Section. [b] Values are approximate due to the overlapping nature of the Ru^{II} and Mn^{II} oxidation potentials. See text for details.
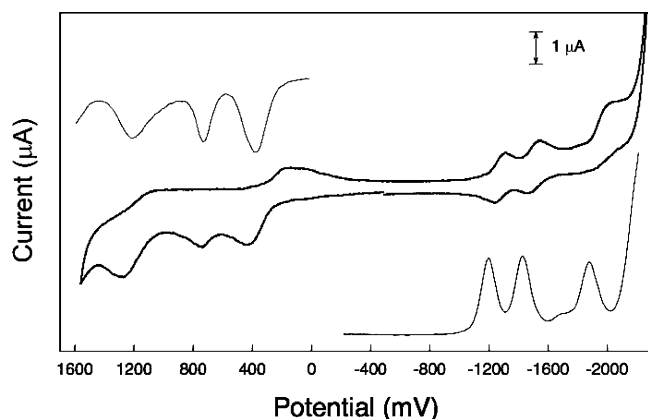
Figure 3. Cyclic voltammogram of [Mn$_2$(L)(mcb)(Ru((CF$_3$)$_2$-bpy)$_2$)](PF$_6$)$_3$ (**4**) in CH$_2$Cl$_2$ solution. Inset graphs are the corresponding differential pulse voltammograms (DPV). All potentials are quoted relative to the ferrocene/ferrocenium couple. See Table 3 for further details.

adducts [Mn$_2$(L)(mcb)(Ru(X$_2$-bpy)$_2$)](PF$_6$)$_3$ (X = CH$_3$ (**3**) CF$_3$ (**4**)) were examined using cyclic (CV) voltammetry; due to the quasi-reversible nature of most of the features, differential pulse voltammograms (DPV) were also recorded. These data are collected in Table 3, with representative CV and DPV traces for complex **4** shown in Figure 3. Complex **1** shows two oxidation waves at +0.08 V and +0.43 V. The simplicity of this molecule allows us to easily assign these two processes to successive oxidations of the Mn^{II} ions, i.e., Mn^{II}-Mn^{II} → Mn^{II}-Mn^{III} (+0.08 V) and Mn^{II}-Mn^{III} → Mn^{III}-Mn^{III} (+0.43 V); their irreversible character is likely a consequence of the lability of Mn^{III} due to the Jahn−Teller distortion associated with this oxidation state. This complex also shows one irreversible wave at −2.00 V that is assigned to the reduction of the bridging mcb ligand. Our data on complex **1** are in good agreement with previously reported potentials for related Schiff-base macrocyclic systems.[34,41]

The cyclic voltammogram of [Mn$_2$(L)(mcb)(Ru((CH$_3$)$_2$-bpy)$_2$)]-(PF$_6$)$_3$ (**3**, Figure S3) reveals a quasi-reversible oxidation at +0.23 V and a broader, somewhat asymmetric feature centered near +0.7 V. The first wave can be ascribed to the first Mn^{II} → Mn^{III} oxidation, where the positive shift relative to complex **1** clearly arises due to ligation of the mcb group to the Ru^{II} center. The broadness of the second feature suggests the presence of multiple unresolved oxidation waves. A comparable shift in the second Mn^{II} oxidation relative to complex **1** would place its potential in the range of 0.6−0.7 V. To estimate where the Ru^{II} → Ru^{III} oxidation might be expected, we prepared and measured the electrochemical properties of [Ru((CH$_3$)$_2$-bpy)$_2$-

(mcbEt)](PF$_6$)$_2$, where mcbEt is the ethyl ester analog of mcb;[42] these data are also reported in Table 3. The presence of a Ru^{II} → Ru^{III} oxidation at +0.79 V in this model system supports the notion the broadened feature we see for complex **3** is, in fact, due to an accidental coincidence of the oxidations of Ru^{II} and the second Mn^{II} ion of the core near +0.7 V.

[Mn$_2$(L)(mcb)(Ru((CH$_3$)$_2$-bpy)$_2$)](PF$_6$)$_3$ also shows two quasi-reversible reductions. Given that the first reduction of complex **1** occurs at −2.0 V, the reductive wave at −1.58 V for complex **3** is clearly associated with ligated bipyridyl groups. The electron-donating properties of the CH$_3$ groups make the peripheral ligands more difficult to reduce relative to the carboxylated bridge, so the first reduction at −1.58 V of complex **3** is assigned to mcb. The reduction at −1.95 V is subsequently assigned to one of the (CH$_3$)$_2$-bpy ligands. Both of these assignments are supported by the data acquired on [Ru-((CH$_3$)$_2$-bpy)$_2$(mcbEt)]$^{2+}$ which exhibits reductions at −1.52 V and −2.00 V attributable to the mcbEt and (CH$_3$)$_2$-bpy ligands, respectively (Table 3). A third feature is also seen for complex **3** but is difficult to interpret due to its proximity to the limiting potential of the solvent.

In the case of [Mn$_2$L(mcb)Ru((CF$_3$)$_2$-bpy)$_2$](PF$_6$)$_3$ (**4**), three oxidations waves are seen: one quasi-reversible process at +0.28 V and two irreversible oxidations at +0.63 V and +1.12 V (Figure 3). The near coincidence of the first wave at +0.28 V with the corresponding data for complex **3** (+0.23 V) suggests a similar assignment, i.e., oxidation of the first Mn^{II} ion. The question of whether to assign the feature at +0.63 V to the Ru^{II} → Ru^{III} or the second Mn^{II} → Mn^{III} oxidation was resolved using electrochemical data acquired on [Ru((CF$_3$)$_2$-bpy)$_2$(mcbEt)]-(PF$_6$)$_2$ (Table 3). The electron-withdrawing nature of the (CF$_3$)$_2$-bpy ligand shifts the oxidation potential of the metal in this compound to +1.14 V as compared to the methylated analog [Ru((CH$_3$)$_2$-bpy)$_2$(mcbEt)](PF$_6$)$_2$. Based on this datum, we can immediately assign the most positive feature in complex **4** at +1.12 V to the Ru^{II} → Ru^{III} oxidation. The observation of the second Mn^{II} → Mn^{III} oxidation in complex **4** at +0.63 V further supports our contention that the broadened feature near +0.7 V in complex **3** was due to an overlap of the Ru^{II} and Mn^{II} oxidations in that compound.

Complex **4** also shows three quasi-reversible reductions, all of which can be assigned to the bipyridine ligands. Here again, we can use data acquired on the Ru^{II} model complexes to aid in the assignments. The first reduction at −1.17 V in complex **4** sits ∼400 mV more positive than the mcb-based reduction in complex **3**: this coupled with the appearance of a similar feature in [Ru((CF$_3$)$_2$-bpy)$_2$(mcbEt)](PF$_6$)$_2$ at −1.15 V clearly indicates

(41) Sun, L.; Raymond, M. K.; Magnuson, A.; LeGourrierec, D.; Tamm, M.; Abrahamsson, M.; Kenez, P. H.; Martensson, J.; Stenhagen, G.; Hammarström, L.; Styring, S.; Akermark, B. *J. Inorg. Biochem.* **2000**, *78*, 15−22.

(42) Electrochemical measurements were attempted on both of the Zn$^{II}_2$ analogs. Unfortunately, we were unable to obtain reasonable quality electrochemical data on these compounds. The underlying reason for this is unclear.

Table 4. Steady-State and Time-Resolved Spectroscopic Data for Complexes **3**−**6** in CH_2Cl_2 Solution

complex	$\lambda_{em\ max}{}^a$ (nm)	τ_{obs} (ns)	$\phi_r{}^b$	$k_r{}^c$ ($\times 10^5$ s^{-1})	$k_{nr}{}^d$ (s^{-1})
[Mn$_2$(L)(mcb)(Ru((CH$_3$)$_2$-bpy)$_2$)](PF$_6$)$_3$ (**3**)	e	0.045 ± 0.005	$<10^{-4}$	$<10\ ^f$	$2.25 \pm 0.25 \times 10^{10}$
[Mn$_2$(L)(mcb)(Ru((CF$_3$)$_2$-bpy)$_2$)](PF$_6$)$_3$ (**4**)	668	5.0 ± 0.1	0.0007^g	1.5 ± 1	$2.0 \pm 0.1 \times 10^8$
[Zn$_2$(L)(mcb)(Ru((CH$_3$)$_2$-bpy)$_2$)](PF$_6$)$_3$ (**5**)	657	1310 ± 50	0.053	0.40 ± 0.05	$0.72 \pm 0.03 \times 10^6$
[Zn$_2$(L)(mcb)(Ru((CF$_3$)$_2$-bpy)$_2$)](PF$_6$)$_3$ (**6**)	664	730 ± 30	0.024	0.33 ± 0.04	$1.3 \pm 0.1 \times 10^6$

^{a} Wavelength accuracy is ± 2 nm. ^{b} Error bars for radiative quantum yields are estimated to be $\pm 10\%$ for values of $\phi_r \geq 10^{-3}$. ^{c} $k_r = k_{obs} \cdot \phi_r$, where $k_{obs} = (\tau_{obs})^{-1}$. ^{d} $k_{nr} = k_{obs} - k_r$. ^{e} The trace emission detected for this compound is due to the presence of a small amount of free [Ru((CH$_3$)$_2$-bpy)$_2$(mcb)]$^+$ present in solutions of complex **3** (cf. 45). ^{f} The lower limit reported here is based on the estimated lower limit for the radiative quantum yield and the fact that no emission from complex **3** was detected. The actual value of k_r for complex **3** is likely to be similar to that of complex **5**. ^{g} Due to the low intensity of the signal, error bars for this value are estimated to be ~50%.

that the first reduction in complex **4** is associated with the more electron-deficient (CF$_3$)$_2$-bpy ligand on the periphery of the Ru polypyridyl fragment.[40] Likewise, the second reduction at −1.40 V is also assigned to a (CF$_3$)$_2$bpy-based reduction based on its similarity to the second reduction at −1.38 V in the model complex. Reduction of the mcb ligand in complex **4** now occurs at −1.85 V, shifted some 300 mV more negative relative to complex **3** due to the fact that it is now the third ligand (as opposed to the first) to undergo reduction.

The electrochemical data just described provides important information concerning the nature of the excited states that will be formed upon excitation of complexes **3**−**6**. Specifically, since the MLCT excited state will preferentially localize on the most easily reduced ligand in a heteroleptic polypyridyl complex,[43] use of either (CH$_3$)$_2$-bpy or its fluorinated analog (CF$_3$)$_2$-bpy as a counterligand will alter the spatial relationship between the excited state of the chromophore and the dinuclear core of the macrocycle. This will have important consequences for interpreting the excited-state dynamics of these systems.

Photophysical Characterization. The photophysical properties of [Mn$_2$(L)(mcb)(Ru((CH$_3$)$_2$-bpy)$_2$)](PF$_6$)$_3$ (**3**) and [Mn$_2$-(L)(mcb)(Ru((CF$_3$)$_2$-bpy)$_2$)](PF$_6$)$_3$ (**4**) were investigated by steady-state and time-resolved spectroscopies in order to assess what influence, if any, the presence of the Mn^{II}$_2$ core has on the photophysics of the Ru^{II}-based excited state. In this regard, the two Zn^{II}$_2$ analogs − [Zn$_2$(L)(mcb)(Ru((CH$_3$)$_2$-bpy)$_2$)](PF$_6$)$_3$ (**5**) and [Zn$_2$(L)(mcb)(Ru((CF$_3$)$_2$-bpy)$_2$)](PF$_6$)$_3$ (**6**) − function as convenient controls insofar as the Zn^{II}$_2$ core is not expected to engage in any excited-state processes such as electron or energy transfer due to its d^{10}-d^{10} configuration. For clarity of presentation, we will discuss the data on each of the two Mn^{II}-containing systems in turn.

A. Photophysical Properties of [Mn$_2$(L)(mcb)(Ru((CH$_3$)$_2$-bpy)$_2$)](PF$_6$)$_3$ (3). The photophysical properties of Ru^{II} polypyridyl complexes have been thoroughly investigated over the past several decades.[44] In general, visible excitation of this class of chromophores results in the formation of a ^{3}MLCT excited state with near unit quantum efficiency. The characteristics of the absorption and emission spectra as well as the excited-state lifetimes of these compounds are reasonably well understood. In accord with our expectations, excitation of [Zn$_2$(L)(mcb)-(Ru((CH$_3$)$_2$-bpy)$_2$)](PF$_6$)$_3$ (**5**) into the ^{1}A$_1$ → ^{1}MLCT absorption at 470 nm in room-temperature CH$_2$Cl$_2$ solution gives rise to a broad emission centered at 657 nm; a plot of this spectrum is given in Figure S4. Based on the electrochemical data discussed in the preceding section, this emission can be assigned to an

excited state localized on the bridging mcb ligand. The spectral profile, lifetime, and radiative quantum yield (Table 4) are all characteristic of ^{3}MLCT-based emission typical for a Ru^{II} polypyridyl complex.

The behavior of [Mn$_2$(L)(mcb)(Ru((CH$_3$)$_2$-bpy)$_2$)](PF$_6$)$_3$ (**3**) stands in stark contrast to the data just described for complex **5**. Specifically, we were unable to detect *any* emission from complex **3** in either steady-state or time-resolved experiments.[45] Based on our detection threshold, this lack of emission indicates a radiative quantum yield for complex **3** of $<10^{-4}$, an attenuation of more than 2 orders of magnitude relative to the Zn^{II}$_2$ model complex. This observation clearly indicates that the excited state of the Ru^{II} chromophore is interacting with the Mn^{II}$_2$ core. Given the low concentration at which the emission measurements were carried out and the subnanosecond time constant necessary to realize such a low radiative quantum yield, intramolecular (as opposed to intermolecular) electron and/or energy transfer between the photoexcited Ru^{II} moiety and the Mn^{II}$_2$ core represent the likely origins for the inferred reactivity. Since the Mn^{II}$_2$ core does not have any visible absorption features, we can immediately rule out significant contributions from Förster energy transfer. However, both electron transfer and Dexter energy transfer are viable excited-state processes in this system. Scheme 3 illustrates the expected consequences of both of these reaction pathways. Electron transfer can only proceed in one direction, namely from the Mn^{II}$_2$ core to the Ru^{II}-based excited state, due to the fact that the Mn^{II}Mn^{II} → Mn^{I}Mn^{II} potential is too negative for the excited state of the Ru^{II} moiety to act as a reductant. Application of the Rehm−Weller equation[46] indicates that electron transfer from the Mn^{II}$_2$ core to the Ru^{II}-based excited state is thermodynamically

(43) The energy of an MLCT excited state can be approximated as the difference between the oxidation potential of the metal and the reduction potential of the ligand. For a given metal complex, then, the lowest energy MLCT state will be associated with the most easily reduced ligand.

(44) (a) Juris, A.; Balzani, V.; Barigelletti, F.; Campagna, S.; Belser, P.; Von Zelewsky, A. *Coord. Chem. Rev.* **1988**, *84*, 85−277. (b) Balzani, V.; Ceroni, P.; Juris, A.; Venturi, M.; Campagna, S.; Puntoriero, F.; Serroni, S. *Coord. Chem. Rev.* **2001**, *219*, 545. (c) Balzani, V.; Juris, A.; Venturi, M.; Campagna, S.; Serroni, S. *Chem. Rev.* **1996**, *96*, 759. (d) Argazzi, R.; Bertolasi, E.; Chiorboli, C.; Bignozzi, C. A.; Itokazu, M. K.; Murakami Iha, N. Y. *Inorg. Chem.* **2001**, *40*, 6885. (e) De Cola, L.; Belser, P.; von Zelewsky, A.; Vogtle, F. *Inorg. Chim. Acta* **2007**, *360*, 775−784.

(45) An extremely weak signal was detected in both the steady-state and the time-resolved emission measurements on complex **3**. A careful analysis of these data (Figure S4), which included a comparison with analogous data acquired for [Ru((CH$_3$)$_2$-bpy)$_2$(mcbEt)](PF$_6$)$_3$, indicated that this residual emission most likely arises from a trace amount of free [Ru((CH$_3$)$_2$-bpy)$_2$-(mcb)]$^+$ present in solutions of complex **3**. The amount of dissociated Ru^{II} species is well below 1% and therefore does not contribute to data from time-resolved absorption experiments.

(46) $\Delta G_0{}^{ET} = E_{1/2}{}^{(D/D+)} - E_{1/2}{}^{(A/A-)} - E_{00}$, where $E_{1/2}{}^{(D/D+)}$ and $E_{1/2}{}^{(A/A-)}$ are the oxidation and reduction potentials of the donor and acceptor, respectively, and E_{00} is the zero-point energy of the excited state (Rehm, D.; Weller, A. *Isr. J. Chem.* **1970**, *8*, 259). Electrochemical potentials used in this calculation are given in Table 3; the value of E_{00} for the ^{3}MLCT state of complex **3** was taken from the spectral fitting analysis of the room-temperature spectrum of complex **5**.

Scheme 3
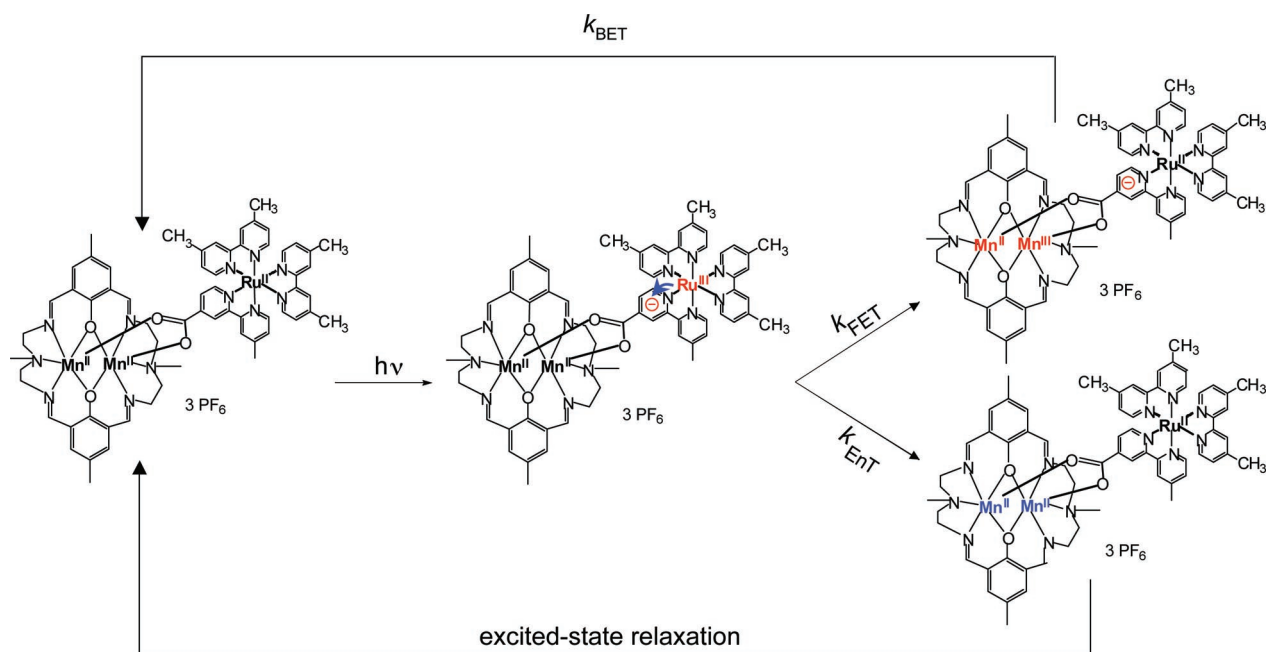
favorable with a driving force of $\Delta G_0^{ET} \approx -0.1$ eV. Dexter transfer, which is an exchange energy-transfer process that can be approximately described as two simultaneous one-electron-transfer events between a donor (Ru^{II*}) and an acceptor (Mn^{II}_2 core), requires the presence of electronic excited state(s) within the acceptor (i.e., Mn^{II}_2) that lie energetically below the excited state of the donor. The existence of multiple low-energy ligand-field states in the excited-state manifold of Mn^{II} serves to satisfy this condition.

To establish which pathway(s) is involved in the excited-state chemistry of complex **3**, we carried out time-resolved absorption measurements in an effort to spectroscopically identify the photoproduct(s) formed following excitation of the Ru^{II} chromophore. Electron transfer will lead to the formation of a charge-separated pair consisting of a $[Ru^{II}((CH_3)_2\text{-bpy})_2\text{-}(mcb^-)]$ fragment and a mixed-valence $Mn^{II}Mn^{III}$ species. The very weak absorptions characteristic of mixed-valence Mn^{II}-Mn^{III} complexes[47] means that identification of the reduced acceptor, i.e., the reductively quenched Ru^{II} polypyridyl fragment, is the best option from an experimental perspective. Electron transfer from the Mn^{II}_2 core should result in partial recovery of the ground-state $^1A_1 \rightarrow {}^1MLCT$ absorption with a time constant corresponding to the rate of electron transfer.[48] In contrast, absorptions associated with the mcb^- species associated with the MLCT excited state should persist during this same time window since it is (nominally) unaffected by the oxidation state of the Ru center. Time-resolved absorption measurements in spectral regions that probe the ground-state

MLCT absorption and the mcb radical anion should therefore give rise to qualitatively different kinetics if an electron-transfer mechanism is operative.

As shown in Scheme 3, Dexter transfer results in the formation of an electronic excited state of the Mn^{II}_2 core and concomitant reformation of the Ru^{II} ground state. As alluded to previously, given the energy of the ^3MLCT state of the Ru^{II} chromophore, absorptions associated with $\{Mn^{II}_2\}*$ will all be ligand-field in nature; the low oscillator strengths associated with these transitions will make them difficult to observe in a transient absorption experiment. Instead, the signature for Dexter transfer will be loss of transient absorption features associated with the ^3MLCT excited state with a time constant equal to the rate of energy transfer. An important consequence of this mechanism is that the observed kinetics should be identical at all probe wavelengths—the MLCT region as well as the mcb^- species—since both components of the Ru^{III}-mcb^- chromophore associated with the charge-transfer excited state are lost simultaneously as a result of energy transfer.

Time-resolved absorption measurements were first carried out on $[Zn_2(L)(mcb)(Ru((CH_3)_2\text{-bpy})_2)](PF_6)_3$ (**5**) in order to identify the key spectral regions associated with the ^3MLCT excited state of the chromophore: these data are shown in Figure 4. Based on spectroelectrochemical measurements,[49] the absorption centered near 380 nm can be attributed to the mcb^- species, whereas the bleach in the 400–500 nm region reflects the loss of the ground-state $^1A_1 \rightarrow {}^1MLCT$ absorption; absorptions further to the red (i.e., $\lambda > 500$ nm) are due to overlapping contributions from mcb^- and an LMCT band which arises upon formation of the MLCT excited state.[49a] These features all exhibit identical single-exponential decay kinetics with time constants that are within experimental error of that obtained from the time-resolved

(47) (a) Diril, H.; Chang, H. R.; Nilges, M. J.; Zhang, X. H.; Potenza, J. A.; Schugar, H. J.; Isied, S. S.; Hendrickson, D. N. *J. Am. Chem. Soc.* **1989**, *111*, 5102–5114. (b) Anderlund, M. F.; Hogblum, J.; Shi, W.; Huang, P.; Eriksson, L.; Weihe, H.; Styring, S.; Akermark, B.; Lomoth, R.; Magnuson, A. *Eur. J. Inorg. Chem.* **2006**, 5033–5047. (c) Gultneh, Y.; Tesema, Y. T.; Yisgedu, T. B.; Butcher, R. J.; Wang, G. B.; Yee, G. T. *Inorg. Chem.* **2006**, *45*, 3023–3033.

(48) In the limit of weak coupling among the bipyridyl ligands, the charge-transfer band of metal polypyridyl complexes can be considered as a superposition of transitions associated with each ligand. Reductive quench-ing of the ^3MLCT excited state will therefore result in recovery of roughly $^2/_3$ of the original oscillator strength of the ground-state absorption.

(49) (a) Damrauer, N. H.; McCusker, J. K. *J. Phys. Chem. A* **1999**, *103*, 8440–8446. (b) Miao, R.; Brewer, K. J. *Inorg. Chem. Commun.* **2007**, *10*, 307–312. (c) Marcaccio, M.; Paolucci, F.; Fontanesi, C.; Fioravanti, G.; Zanarini, S. *Inorg. Chim. Acta* **2007**, *360*, 1154–1162. (d) Fabre, M.; Jaud, J.; Hliwa, M.; Launay, J.-P.; Bonvoisin, J. *Inorg. Chem.* **2006**, *45*, 9332–9345.
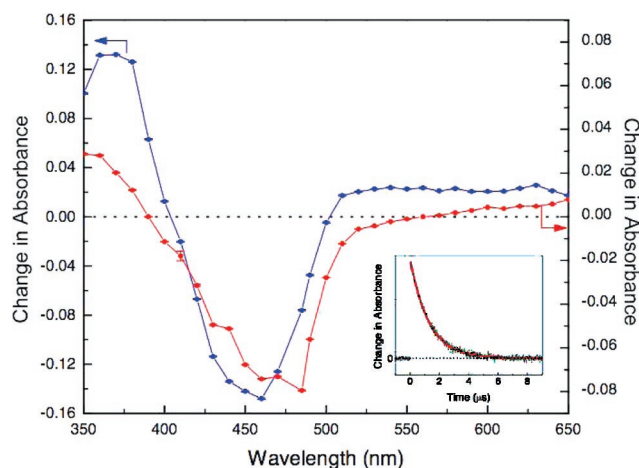
Figure 4. Nanosecond time-resolved differential absorption spectra for [Zn$_2$-(L)(mcb)(Ru((CH$_3$)$_2$-bpy)$_2$)](PF$_6$)$_3$ (**5,** blue solid line) and [Zn$_2$(L)(mcb)-(Ru((CF$_3$)$_2$-bpy)$_2$)](PF$_6$)$_3$ (**6,** red solid line) obtained in room-temperature CH$_2$Cl$_2$ solution following excitation at 470 nm. The spectra were constructed from the amplitudes of fits of the single-wavelength kinetic data. The inset shows an example of one of these kinetic traces for complex **5** at $\lambda_{probe} = 380$ nm ($\tau_{obs} = 1.3$ μs).

Figure 5. Femtosecond time-resolved absorption data for [Mn$_2$(L)(mcb)-(Ru((CH$_3$)$_2$-bpy)$_2$)](PF$_6$)$_3$ (**3**) at $\lambda_{probe} = 490$ nm (red) and $\lambda_{probe} = 550$ nm (blue) following ~100 fs excitation at $\lambda_{pump} = 470$ nm. The solid lines through the data correspond to fits to a single-exponential decay model with $\tau_{obs} = 45 \pm 5$ ps. The slight mismatch between the data and the fit evident at early times for $\lambda_{probe} = 490$ nm (red) is due to a small amount of laser scatter. The inset shows analogous transient absorption data for [Zn$_2$(L)(mcb)(Ru((CH$_3$)$_2$-bpy)$_2$)](PF$_6$)$_3$ (**5**) at $\lambda_{probe} = 550$ nm. See text for further details.

emission measurements described previously (Figure 4, inset). Our observations on complex **5** are thus indicative of simple ground-state recovery due to decay of the ^{3}MLCT excited state, as expected for this model complex.

The lack of emission from [Mn$_2$(L)(mcb)(Ru((CH$_3$)$_2$-bpy)$_2$)]-(PF$_6$)$_3$ (**3**) strongly suggests that the excited-state dynamics of this system are occurring on a picosecond (or faster) time scale. Accordingly, we carried out transient absorption measurements on complex **3** using femtosecond time-resolved absorption spectroscopy. Given that additional dynamics can be discerned on ultrafast time scales that are not resolvable using nanosecond spectroscopy,[50] we performed analogous measurements on [Zn$_2$-(L)(mcb)(Ru((CH$_3$)$_2$-bpy)$_2$)](PF$_6$)$_3$ (**5**) as a control. Data were acquired on both compounds following ~100 fs excitation at 470 nm. Both full-spectrum data and single-wavelength kinetics at multiple probe wavelengths were collected; in Figure 5 are shown representative single-wavelength kinetic traces for complex **3** at $\lambda_{probe} = 490$ nm and $\lambda_{probe} = 550$ nm as well as for the Zn$^{II}_2$ model complex at $\lambda_{probe} = 550$ nm (inset). The kinetics for complex **3** at all probe wavelengths examined (330–700 nm) can be modeled by a single-exponential decay back to baseline with a time constant of $\tau_{obs} = 45 \pm 5$ ps. The data for complex **5** do not reveal any dynamics in this same time window, indicating that the kinetics observed for complex **3** are indeed associated with the presence of the Mn$^{II}_2$ core. The time constant of 45 ± 5 ps corresponds to a rate that is more than a factor of 10^4 faster than the decay of the ^{3}MLCT state of complex **5**. This explains why no emission was detected for complex **3**: the dynamics, which indicate reactivity from the thermalized ^{3}MLCT state,[51] would be expected to lead to a corresponding decrease (i.e., ~10^4) in the emission quantum yield from that state. In terms of the quenching mechanism, the data in Figure 5 reveal that spectral regions probing different components of the excited-state moiety are exhibiting identical kinetics that return completely to the baseline. These observations are strongly suggestive of the simultaneous disappearance
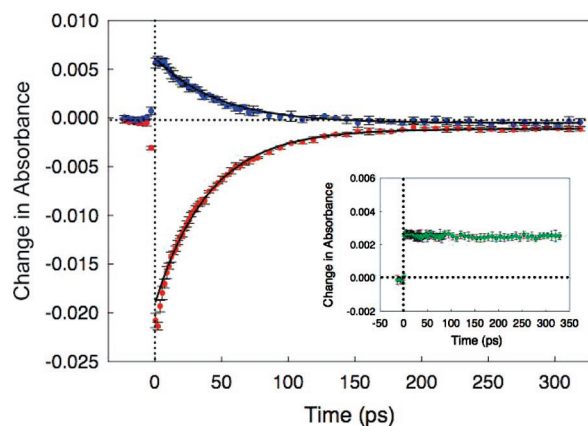
of both components of the Ru^{III}-mcb$^-$ species formed upon excitation, consistent with energy transfer to the dimanganese core.

Although the analysis presented above reflects the typical rationale employed when direct detection of the electronically excited acceptor is not possible, there is another mechanistic scenario that must be considered. The detection of a transient absorption signal necessitates the buildup of a sufficient concentration of the excited-state species being probed: this was an implicit assumption in the preceding discussion as to what signals we should expect in the case of electron transfer for complex **3**. This condition can be compromised if the rate at which the excited-state species decays is significantly faster than its rate of formation (i.e., $k_{BET} \gg k_{FET}$ in Scheme 3). In this circumstance, the kinetics reflected by the data shown in Figure 5 would correspond to the forward electron-transfer process (k_{FET}) as the rate-limiting step in the reaction sequence, but qualitatively the spectroscopic data would be indistinguishable from Dexter transfer because the charge-separated species is disappearing immediately upon formation. The driving force for the forward reaction in complex **3** is −0.1 eV; however, back-electron transfer is considerably more exothermic (ΔG_0^{BET} = −1.8 eV). The significance of this difference will depend on the relative magnitudes of the reorganization energies associated with each reaction, but the substantial increase in the driving force coupled with the fact that the electron donor for the back-reaction (mcb$^-$) is directly adjacent to the acceptor (Mn^{II}Mn^{III}) makes the scenario just described a distinct possibility. We therefore cannot definitively distinguish between Dexter and rapid, sequential electron transfer in this system on the basis of these data alone.

B. Photophysics of [Mn$_2$(L)(mcb)(Ru((CF$_3$)$_2$-bpy)$_2$)](PF$_6$)$_3$ (4). For complex **4** we have a situation analogous to that for complex **3**, namely the possibility of both electron and Dexter

(50) McCusker, J. K. *Acc. Chem. Res.* **2003,** *36,* 878–887.

(51) Formation of the ^{3}MLCT excited state following ^{1}A$_1$ → ^{1}MLCT excitation occurs on a subpicosecond time scale. See: Damrauer, N. H.; Cerullo, G.; Yeh, A.; Boussie, T. R.; Shank, C. V.; McCusker, J. K. *Science* **1997,** *275,* 54–57.
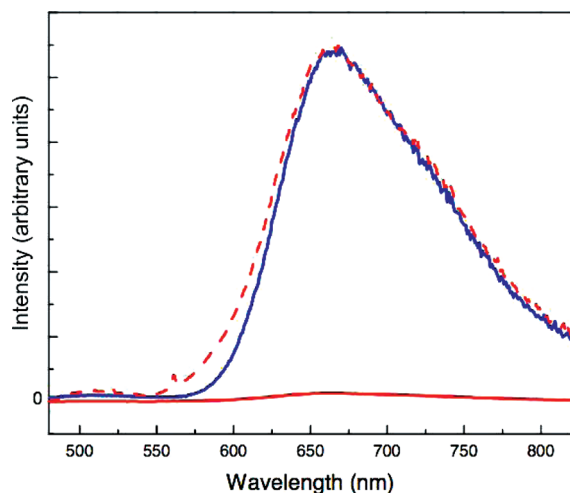
Figure 6. Corrected emission spectra of [Zn$_2$(L)(mcb)(Ru((CF$_3$)$_2$-bpy)$_2$)]-(PF$_6$)$_3$ (**6**, blue) and [Mn$_2$(L)(mcb)(Ru((CF$_3$)$_2$-bpy)$_2$)](PF$_6$)$_3$ (**4**, red) in room-temperature CH$_2$Cl$_2$ solution following excitation at 470 nm. The dashed line corresponds to the emission spectrum of complex **4** normalized to the intensity of complex **6** for comparative purposes. See Table 4 for further details.

Figure 7. Time-resolved emission data for [Zn$_2$(L)(mcb)(Ru((CF$_3$)$_2$-bpy)$_2$)]-(PF$_6$)$_3$ (**6**, black) and [Mn$_2$(L)(mcb)(Ru((CF$_3$)$_2$-bpy)$_2$)](PF$_6$)$_3$ (**4**, blue) in room-temperature CH$_2$Cl$_2$ solution at 668 nm following excitation at 470 nm. These data were acquired on a nanosecond time-resolved spectrometer; the inset shows analogous data on complex **4** acquired via TCSPC with ~20 ps resolution. The red solid lines correspond to fits of the data to single-exponential decay kinetics with $\tau_{obs} = 5.0 \pm 0.1$ ns and 730 ± 30 ns for complexes **4** and **6**, respectively.

energy transfer between the Ru^{II} chromophore and Mn$^{II}_2$ core. One important difference particularly with regard to an electron-transfer mechanism stems from the spatial characteristics of the system: whereas the reaction corresponding to k_{FET} in complex **4** traverses a path similar to that of complex **3** (a notable exception being the electronic configuration of the bridge), the back-reaction in complex **4** would now proceed from the periphery of the Ru-polypyridyl fragment as opposed to the ligand adjacent to the Mn$^{II}_2$ core. The substitution of CF$_3$ for CH$_3$ also impacts the driving force for the electron transfer, with the more electron-deficient Ru^{II} center of complex **4** contributing to an increase in the free energy change for reductive quenching of the ^{3}MLCT state to ca. -0.43 eV; the driving force for the back-reaction is correspondingly smaller with $\Delta G_0^{BET} = -1.45$ eV. Energy-transfer dynamics should also be affected by repositioning of the excited state away from the bridging mcb group vis-à-vis slowing the rate of Dexter transfer due to the increase in effective donor−acceptor distance. We therefore anticipate substantial differences in the excited-state properties of complex **4** relative to complex **3** as a result of this synthetic modification.

The experiments carried out on [Mn$_2$(L)(mcb)(Ru((CF$_3$)$_2$-bpy)$_2$)](PF$_6$)$_3$ (**4**) exactly mirror those performed on complex **3**; the Zn^{II} analog of this system, [Zn$_2$(L)(mcb)(Ru((CF$_3$)$_2$-bpy)$_2$)](PF$_6$)$_3$ (**6**), was also examined. The steady-state emission spectra of both of these complexes are shown in Figure 6. As expected, complex **6** exhibits emission characteristic of a ^{3}MLCT state of a Ru^{II} polypyridyl complex. The emission is slightly red-shifted as compared to complex **5**, reflecting the lower energy of the (CF$_3$)$_2$bpy-based excited state. In contrast to the lack of emission from complex **3**, [Mn$_2$(L)(mcb)(Ru-((CF$_3$)$_2$-bpy)$_2$)](PF$_6$)$_3$ (**4**) exhibits a weak but nevertheless measurable emission with a spectral profile identical to that of [Zn$_2$(L)(mcb)(Ru((CF$_3$)$_2$-bpy)$_2$)](PF$_6$)$_3$ (**6**). The emission from complex **4** is still significantly quenched relative to its Zn$^{II}_2$ analog as reflected in both its reduced radiative quantum yield (Table 4) and excited-state lifetime of 5.0 ± 0.1 ns (Figure 7). This represents a reduction of more than 2 orders of magnitude
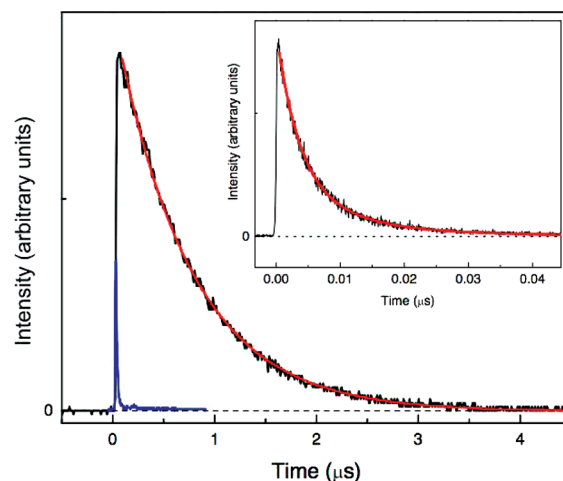
relative to [Zn$_2$(L)(mcb)(Ru((CF$_3$)$_2$-bpy)$_2$)](PF$_6$)$_3$ (**6**) but is still 2 orders of magnitude longer than the 45 ps lifetime observed for [Mn$_2$(L)(mcb)(Ru((CH$_3$)$_2$-bpy)$_2$)](PF$_6$)$_3$ (**3**).

Transient absorption data were acquired on the nanosecond time scale for [Mn$_2$(L)(mcb)(Ru((CF$_3$)$_2$-bpy)$_2$)](PF$_6$)$_3$ (**4**) across a wide range of probe wavelengths; representative traces are shown in Figure 8. In all cases and at all wavelengths, the data exhibited complete recovery back to the baseline. In particular, we can see that both the bleach of the ground-state ^{1}A$_1$ → ^{1}MLCT absorption ($\lambda_{probe} = 490$ nm) as well as the absorption of the (CF$_3$)$_2$bpy-based radical anion ($\lambda_{probe} = 370$ nm) evolve with identical kinetics back to the ground state. This is again consistent with an energy-transfer mechanism in which the Ru^{III}-(CF$_3$)$_2$-bpy$^-$ species comprising the ^{3}MLCT excited state undergoes relaxation back to its ^{1}A$_1$ ground state concomitant with formation of a ligand-field excited state(s) in the dimanganese core. Nevertheless, the significant driving force for back-electron transfer again raises the possibility of rapid charge-recombination. The situation with complex **4** is somewhat less problematic in that the increase in donor−acceptor distance for the back-reaction should substantially reduce k_{BET}, but there still exists a degree of ambiguity that cannot be easily removed without additional information.

Dexter versus Sequential Electron Transfer: Variable-Temperature Spectroscopies. Absent direct detection of photoproducts, we are faced with a classic problem in excited-state chemistry of trying to distinguish between electron and energy transfer. Although the observations from time-resolved absorption spectroscopy strongly suggest Dexter transfer from the ^{3}MLCT excited states in both complex **3** and complex **4**, significant driving forces for charge-recombination and issues pertaining to the spatial localization of the excited states involved compelled us to try to obtain more definitive evidence for either mechanistic scenario.

Regardless of whether the reaction we are observing is electron or energy transfer, the same semiclassical formalism governing the rates of nonradiative processes can be applied:
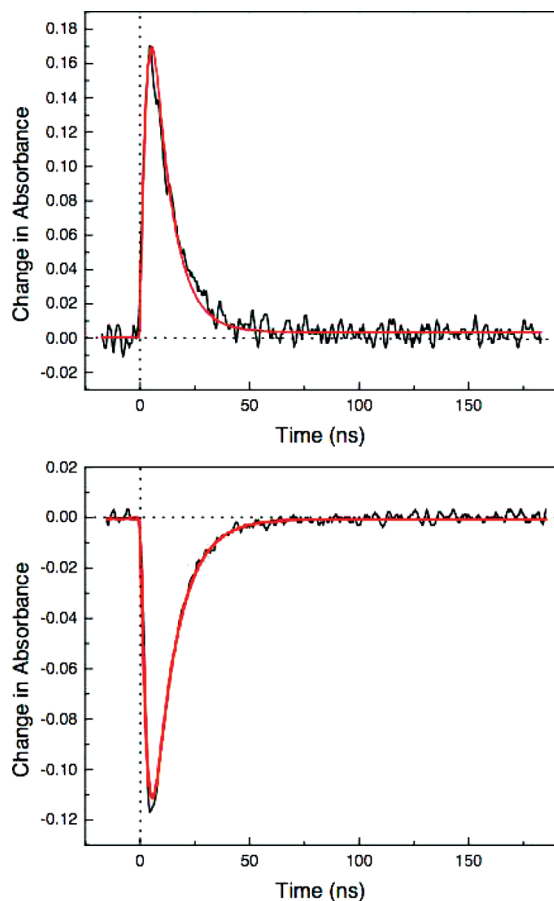
Figure 8. Nanosecond time-resolved absorption data for [Mn$_2$(L)(mcb)-(Ru((CF$_3$)$_2$-bpy)$_2$)](PF$_6$)$_3$ (**4**) in room-temperature CH$_2$Cl$_2$ solution at λ_{probe} = 370 nm (top) and λ_{probe} = 490 nm (bottom) following excitation at 470 nm. The red lines represent fits of the data to single-exponential decay models with τ_{obs} = 5 ± 1 ns convolved with the instrument response function of the spectrometer. The slight positive offset from baseline in the data at λ_{probe} = 370 nm is due to a small degree of baseline instability.

$$k_{nr} = \frac{4\pi^2}{h} \cdot |H_{ab}|^2 \cdot \frac{1}{\sqrt{4\pi\lambda k_B T}} \cdot \exp\left(-\frac{(\Delta G_0 + \lambda)^2}{4\lambda k_B T}\right) \quad (2)$$

In this well-known expression, ΔG_0 and λ correspond, respectively, to the free energy change and reorganization energy associated with the reaction, while H_{ab} represents the electronic coupling between the donor and the acceptor. A key factor in helping to distinguish between energy and electron transfer is the magnitude of λ. Electron-transfer reactions generally have reorganizations energies on the order of 1−2 eV depending on the nature of the reactants (inner-sphere contributions) and the solvent (outer-sphere); in contrast, energy-transfer processes are expected to exhibit considerably smaller values for λ due to the lack of a formal net transfer of charge associated with this process.[52] Based on the form of eq 2, it can be seen that variable-temperature rate data can in principle afford a value for λ and thereby provide critical information to help distinguish between Dexter transfer and the rapid back-electron-transfer mechanism described in the previous section.

[Mn$_2$(L)(mcb)(Ru((CF$_3$)$_2$-bpy)$_2$)](PF$_6$)$_3$ (4). Variable-temperature time-resolved emission data of a CH$_2$Cl$_2$ solution of complex **4** are plotted in Figure 9. In addition to the quenching process of interest, relaxation of the ^{3}MLCT excited state is expected to exhibit its own intrinsic temperature dependence.
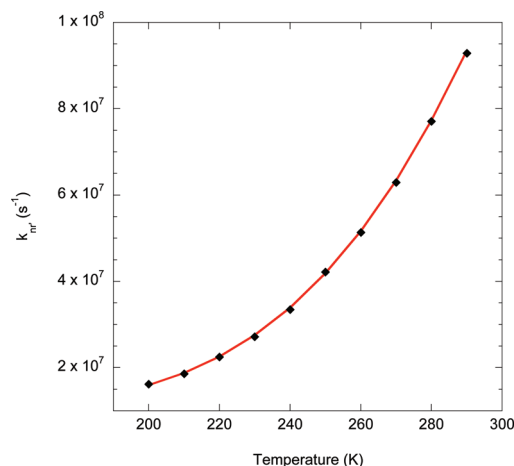
Figure 9. Variable-temperature time-resolved emission data for [Mn$_2$(L)-(mcb)(Ru((CF$_3$)$_2$-bpy)$_2$)](PF$_6$)$_3$ (**4**) in CH$_2$Cl$_2$ solution at λ_{probe} = 660 nm following excitation at λ_{pump} = 470 nm. The data are plotted as the nonradiative rate constant for quenching of the ^{3}MLCT excited state of complex **4**, $k_{nr'} = k_{obs}^{(4)} - k_{obs}^{(6)}$, where $k_{obs}^{(6)}$ corresponds to the observed rate constant for decay ($k_{obs} = k_r + k_{nr}$) for the Zn-containing analog [Zn$_2$-(L)(mcb)(Ru((CF$_3$)$_2$-bpy)$_2$)](PF$_6$)$_3$ (**6**) at each temperature (Figure S5). The solid red line corresponds to a fit of the data to eq 3 with k_0 = 1.065 ± 0.05 × 10^7 s^{-1}, A = 3.7 ± 0.5 × 10^{10} s^{-1}, and $\Delta E^{\ddagger}$ = 1230 ± 30 cm^{-1}. See text for further details.

We therefore also acquired variable-temperature data on [Zn$_2$-(L)(mcb)(Ru((CF$_3$)$_2$-bpy)$_2$)](PF$_6$)$_3$ (**6**) over the same temperature range (Figure S5); the data in Figure 9 have been corrected for this underlying contribution.[53] Our initial efforts involved fitting the data on complex **4** to eq 2 (Figure S6). Although this analysis was able to qualitatively reproduce the observed temperature dependence of the rate of excited-state decay, the overall agreement is not particularly good. A significantly better fit of the data was obtained using eq 3

$$k_{nr} = k_0 + A \cdot \exp\left(-\frac{\Delta E^{\ddagger}}{k_B T}\right) \quad (3)$$

where k_0 is a temperature-independent component to the observed nonradiative decay dynamics and the Arrhenius factor represents a barrier to additional state(s) that give rise to thermally activated decay channels. The fit in Figure 9 corresponds to values of k_0 = 1.065 ± 0.05 × 10^7 s^{-1}, A = 3.7 ± 0.5 × 10^{10} s^{-1}, and $\Delta E^{\ddagger}$ = 1230 ± 30 cm^{-1}.

Equation 3 is commonly used to describe the temperature dependence of ^{3}MLCT relaxation in Ru^{II} polypyridyl complexes,[54] but the physical interpretation of the fitting parameters varies depending upon the nature of the system under study. For example, the activation energy of the Arrhenius term has been associated with low-lying ligand-field excited state(s)[54a]

(52) (a) Barigelletti, F.; Flamigni, L.; Guardigli, M.; Juris, A.; Beley, M.; Chodorowski-Kimmes, S.; Collin, J.-P.; Sauvage, J.-P. *Inorg. Chem.* **1996**, *35*, 136−142. (b) Hamada, T.; Tanaka, S.; Koga, H.; Sakai, Y.; Sakaki, S. *J. Chem. Soc., Dalton Trans.* **2003**, 692−698. (c) Liard, D. J.; Kleverlaan, C. J.; Vlcek, A. *Inorg. Chem.* **2003**, *42*, 7995−8002. (d) Indelli, M. T.; Bignozzi, C. A.; Harriman, A.; Schoonover, J. R.; Scandola, F. *J. Am. Chem. Soc.* **1994**, *116*, 3768−3779.

(53) The rate constant for quenching in complex **4** is given by $k_{nr'} = k_{obs}^{(4)} - k_{obs}^{(6)}$, where $k_{obs}^{(4)}$ and $k_{obs}^{(6)}$ are the observed rate constants for complexes **4** and **6**, respectively.

(54) (a) Thompson, D. W.; Fleming, C. N.; Myron, B. D.; Meyer, T. J. *J. Phys. Chem.* **2007**, *111*, 6930−6941, and references therein. (b) Cooley, L. F.; Larson, S. L.; Elliot, C. M.; Kelley, D. F. *J. Phys. Chem.* **1991**, *95*, 10694−10700. (c) Larson, S. L.; Cooley, L. F.; Elliot, C. M.; Kelley, D. F. *J. Am. Chem. Soc.* **1992**, *114*, 9504−9509.

as well as additional charge-transfer states within the MLCT manifold.[54b,c] In this regard, the data acquired on the model complex $[Zn_2(L)(mcb)(Ru((CF_3)_2\text{-bpy})_2)](PF_6)_3$ (**6**) provide us with important information concerning the physical origin of these terms for this system. The variable-temperature relaxation data for complex **6** are well represented by eq 3 with values of $k_0 = 1.13 \pm 0.05 \times 10^6$ s^{-1}, $A = 1.0 \pm 0.9 \times 10^8$ s^{-1}, and $\Delta E^{\ddagger} = 1200 \pm 200$ cm^{-1}. Given the known electronic structure of this compound, we can immediately ascribe the temperature-independent rate constant k_0 to the relaxation dynamics of the ^{3}MLCT state localized on the peripheral (CF$_3$)$_2$-bpy ligand. The Arrhenius term is not as straightforward to interpret since it can in principle reflect a convolution of several factors, chief among these being the aforementioned ligand-field excited state-(s) of the Ru^{II} chromophore and, in the present case, the charge-transfer manifold associated with the mcb bridging ligand.[54b,c] The magnitude of $\Delta E^{\ddagger}$ deduced for complex **6** is significantly smaller than what has typically been observed for the ^{3}MLCT– ligand-field gap in this class of compounds:[54a,55] this fact coupled with a lack of propensity for photodecomposition in room-temperature solution suggests that thermal activation of ligand-field states is not the primary origin of the temperature-dependent response for complex **6**.[56]

A more compelling argument for assigning the Arrhenius term to population of the mcb-localized charge-transfer manifold comes from a comparison of the fitting parameters for complexes **6** and **4**. The fact that the values deduced for $\Delta E^{\ddagger}$ are identical within experimental error for these isostructural compounds strongly implies that both compounds are sampling the same barrier. In contrast, we note that the pre-exponential terms for complexes **4** and **6** differ by more than 2 orders of magnitude (3.7×10^{10} s^{-1} versus 1.0×10^8 s^{-1} for complexes **4** and **6**, respectively). Interpretation of the specific value we obtained for complex **4** will be taken up shortly, but in a general sense the pre-exponential term in an Arrhenius expression can be viewed as the rate constant expected in the limit of a barrierless reaction from the state associated with $\Delta E^{\ddagger}$. Whether the mcb ligand bridges to a Zn$^{II}_2$ or Mn$^{II}_2$ core should have little if any effect on the intrinsic reactivity of ligand-field states of the $[Ru((CF_3)_2\text{-bpy})_2(mcb)]^+$ chromophore. In other words, the Arrhenius fit should yield similar values for the pre-exponential terms for complexes **4** and **6** if $\Delta E^{\ddagger}$ corresponded to the ^{3}MLCT–ligand-field gap in this system. This is clearly not the case. We therefore attribute the temperature dependence of the relaxation dynamics of complex **6** to thermal population of the ^{3}MLCT state associated with the mcb bridge.

These assignments provide the basis for interpreting the variable-temperature data on $[Mn_2(L)(mcb)(Ru((CF_3)_2\text{-bpy})_2)]$-$(PF_6)_3$ (**4**). As with complex **6**, we can ascribe the k_0 term in complex **4** to dynamics originating from the (CF$_3$)$_2$bpy-based ^{3}MLCT excited state and thus to the quenching process associated with the peripheral ligand of the Ru^{II} chromophore. The pre-exponential value of $3.7 \pm 0.5 \times 10^{10}$ s^{-1} for the Arrhenius term for complex **4** is comparable to the time constant observed for excited-state quenching of [Mn$_2$(L)(mcb)(Ru-

$((CH_3)_2\text{-bpy})_2)](PF_6)_3$ (**3**) ($k_{obs} = 2.2 \pm 0.3 \times 10^{10}$ s^{-1}). Since the dynamics associated with complex **3** are known to arise from a mcb-based excited state, we view this correlation as lending strong additional support to our assignment of the origin of this pathway in terms of thermal population of the mcb-based charge-transfer state. This analysis indicates that we are dealing with two modes of reactivity in complex **4**, one associated with the peripheral (CF$_3$)$_2$-bpy ligand and a second subsequent to thermal population of the bridge-localized ^{3}MLCT state.

The original intention of acquiring variable-temperature data on complex **4** was to glean insight into the magnitude of the reorganization energy associated with the quenching process. Elliot and Kelley in particular[54b,c] have pointed out that the presence of spatially distinct, thermally accessible states can have a significant impact on the relaxation dynamics of donor/acceptor assemblies and therefore on the physical interpretation of any temperature dependence in reaction rate constants. Our analysis of the data on complex **4** is certainly consistent with this picture: the temperature dependence of the excited-state dynamics of complex **4** is clearly dominated by the intrinsic asymmetry of the assembly. This makes a direct determination of λ difficult, but we can nevertheless use our analysis of the data shown in Figure 9 to estimate a range of possible values that λ can take on in order to be consistent with the observed reactivity of complex **4** and evaluate those results in the context of the two mechanistic scenarios under consideration.

Recall that in the rapid back-electron-transfer model, the reaction we would be monitoring is the slow step, i.e., the formation of the charge-separated species. This reaction would proceed with a driving force of $\Delta G_0 = -0.43$ eV based on the electrochemical and steady-state emission data described previously. To ensure the applicability of this value over the temperature range covered by the data shown in Figure 9, we carried out electrochemical measurements on complex **4** from room temperature down to 210 K. Variations in both the oxidative and reductive potentials were less than 0.1 V and moreover did not exhibit any systematic trend within this range. This is consistent with the observations of Hammarström and co-workers who noted a similar invariance in the electrochemistry of related systems from 10 °C to 60 °C,[8b] indicating that the driving force for electron transfer is relatively constant over the range of temperature being considered.

The absence of a measurable barrier associated with the quenching of the (CF$_3$)$_2$bpy-based excited state indicates that reactivity is occurring via a tunneling mechanism and/or is proceeding near the barrierless limit of the reaction. In the latter case, an electron-transfer-based mechanism would require a value of λ on the order of 0.4–0.5 eV. This is well below what one typically associates with such a reaction even in a relatively nonpolar solvent such as CH$_2$Cl$_2$. A similar inference is more difficult to draw for the temperature-dependent process since the barrier associated with accessing the mcb-based excited state dominates the Arrhenius term. The fact that the same value of $\Delta E^{\ddagger}$ was found for both complexes **4** and **6** implies that the barrier for the second step in complex **4** (i.e., reaction with the Mn$^{II}_2$ core) is substantially less than 1200 cm^{-1}, an assertion that is supported by the fact that the rate constant given by the pre-exponential term for complex **4** is less than a factor of 2 larger than the room-temperature rate directly measured for complex **3** (vide supra). Using 500 cm^{-1} as a conservative

(55) Barqawi, K. ep.; Llobet, A.; Meyer, T. J. *J. Am. Chem. Soc.* **1988**, *110*, 7751−7759, and references therein.

(56) Although photosubstitution chemistry is often associated with thermally accessible ligand-field excited states in charge-transfer complexes, its absence does not necessarily discount the existence of such states. See: Thompson, D. W.; Wishart, J. F.; Brunschwig, B. S.; Sutin, N. *J. Phys. Chem. A* **2001**, *105*, 8117−8122.

estimate for this second barrier, application of eq 4

$$\Delta G^{\ddagger} = \frac{(\Delta G_0 + \lambda)^2}{4\lambda} \qquad (4)$$

indicates that the reorganization energy for quenching the mcb-based excited state in complex **4** can be no larger than 1 eV in order to be consistent with our variable-temperature data; this upper limit drops to less than 0.75 eV if a more realistic value of 200 cm^{-1} is employed.[57]

We carried out two additional sets of experiments on this system in an effort to further support our conclusions. First, time-resolved absorption data were collected over the same temperature range as the emission data shown in Figure 9. These measurements did not reveal any new signals suggesting the formation of electron-transfer photoproducts: at all temperatures and at all probe wavelengths monitored, transient signals were found to return completely to baseline in a manner similar to what was seen at room temperature (i.e., Figure 8). In addition to these solution-phase data, we also acquired steady-state and time-resolved emission data on complex **4** below the glass-to-fluid transition of the solvent (Figure S7). The data revealed that the photophysics of this compound are insensitive to the formation of a glass in that neither the time-resolved nor steady-state measurements indicated any discontinuous change in emissive properties of complex **4**: this is contrary to what is typically observed for an electron-transfer process.[58] We believe the totality of these results firmly establishes Dexter transfer as the dominant quenching mechanism following charge-transfer-state formation in [Mn$_2$(L)(mcb)(Ru((CF$_3$)$_2$-bpy)$_2$)](PF$_6$)$_3$.

With this assignment in hand, we can investigate further the parameters governing Dexter transfer in this system. Of particular interest is the magnitude of H_{ab}, which defines the superexchange interaction responsible for energy transfer. In the limit of a barrierless reaction, H_{ab} can be evaluated from eq 2 as

$$H_{ab} = \left[\frac{k_{nr} \cdot h \cdot (4\pi\lambda k_B T)^{1/2}}{4\pi^2}\right]^{1/2} \qquad (5)$$

where k_{nr} is the rate constant for energy transfer and λ is its associated reorganization energy; in the case of complex **4**, k_{nr} corresponds to k_0 from the fit of the variable-temperature relaxation data in Figure 9. Ordinarily the value for λ is derived directly from the temperature dependence of the rate of reaction given a value for ΔG_0. This is clearly not a viable approach in the present case due to the complicated nature of the temperature dependence of this system and the fact that the energy of the acceptor state(s) is not easily determined. Fortunately, the availability of our Zn model complexes affords us the means to obtain a reasonable estimate of λ. Dexter transfer corresponds

---

(57) The difference between the pre-exponential rate constant for complex **4** and the rate constant for complex **3** measured at room temperature implies a barrier in the range of 100−200 cm^{-1}. In this regard it should be noted that complex **3** is also expected to exhibit a temperature-dependent contribution to the overall reaction rate due to the thermal population of the (CH$_3$)$_2$-bpy-based charge-transfer manifold. Given that these states are associated with the peripheral ligands, their intrinsic quenching rates will be substantially slower than the mcb-based kinetics and therefore should not significantly impact k_{obs}.

(58) The lack of emission in the low-temperature glass is strongly suggestive of an energy-transfer mechanism but is not necessarily definitive. For a more detailed discussion of the issues surrounding electron transfer in rigid media, see: Chen, P. Y.; Meyer, T. J. *Chem. Rev.* **1998**, *98*, 1439−1477.
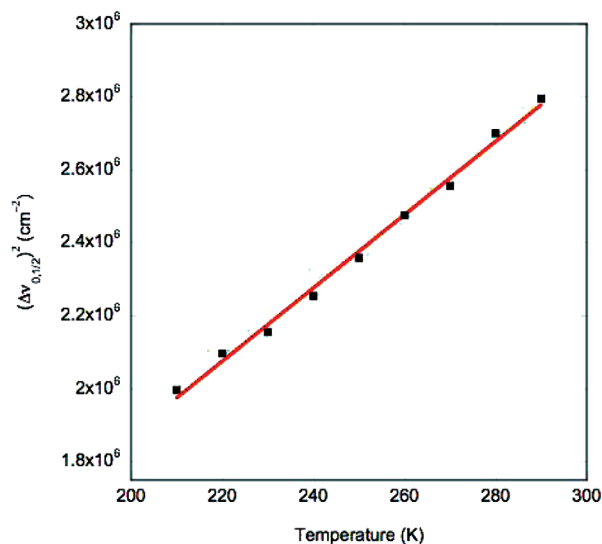
Figure 10. Plot of $(\Delta\nu_{0,1/2})^2$ versus temperature for [Zn$_2$(L)(mcb)(Ru-((CF$_3$)$_2$-bpy)$_2$)](PF$_6$)$_3$ (**6**), where $\Delta\nu_{0,1/2}$ is the full-width-at-half-maximum of the 0−0 vibronic component derived from fits of the steady-state emission spectra (Figure S8). The slope is proportional to the sum of the outer-sphere and low-frequency mode reorganization energies for ^{3}MLCT relaxation (eq 7). See text for further details.

to the collapse of the ^{3}MLCT state of the Ru^{II} chromophore (i.e., the Ru^{III}-(CF$_3$)$_2$-bpy$^-$ species) and concomitant formation of a ligand-field excited state(s) within the Mn$^{II}_2$ core. The total reorganization energy for this reaction can therefore be approximated as the sum of the reorganization energies of these two individual processes. As Meyer and co-workers have shown,[32,59−61] the emission spectra of metal polypyridyl complexes contain information related to the inner- and outer-sphere reorganization energies of the ^{3}MLCT states from which they arise. Such spectral fitting analyses can in the most favorable circumstances be used to model the temperature dependence of nonradiative decay from these states.[32] In the present case, fitting of the ^{3}MLCT emission of [Zn$_2$(L)(mcb)(Ru((CF$_3$)$_2$-bpy)$_2$)](PF$_6$)$_3$ as a function of temperature will provide us with an estimate λ for relaxation of the ^{3}MLCT state of complex **4** due to Dexter transfer.

Variable-temperature steady-state emission spectra for complex **6** were acquired in CH$_2$Cl$_2$ solution and are plotted in Figure S8. Following the single-mode analysis described in detail by Claude and Meyer,[32] the emission spectra ($I(\bar{\nu})$) were fit to eq 6

$$I(\bar{\nu}) = \sum_{\nu_M=0}^{5} \left\{ \left(\frac{E_{00} - \nu_M \hbar\omega_M}{E_{00}}\right)^3 \cdot \left(\frac{S_M^{\nu_M}}{\nu_M!}\right) \times \right.$$
$$\left. \exp\left(-4(\ln 2)\left(\frac{\bar{\nu} - E_{00} + \nu_M \hbar\omega_M}{\Delta\bar{\nu}_{0,1/2}}\right)^2\right)\right\} \qquad (6)$$

to yield values for the zero-point energy of the ^{3}MLCT state

---

(59) (a) Kober, E. M.; Caspar, J. V.; Lumpkin, R. S.; Meyer, T. J. *J. Phys. Chem.* **1986**, *90*, 3722−3734. (b) Graff, D.; Claude, J.-P.; Meyer, T. J. *Adv. Chem. Ser.* **1997**, *253*, 183−198.

(60) (a) Murtaza, Z.; Graff, D. K.; Zipp, A. P.; Worl, L. A.; Jones, W. E., Jr.; Bates, W. D.; Meyer, T. J. *J. Phys. Chem.* **1994**, *98*, 10504−10513. (b) Barqawi, K. R.; Murtaza, Z.; Meyer, T. J. *J. Phys. Chem.* **1991**, *95*, 47−50. (c) Thompson, D. W.; Schoonover, J. R.; Meyer, T. J.; Argazzi, R.; Bignozzi, C. A. *J. Chem. Soc., Dalton Trans.* **1999**, 3729−3734.

(E_{00}), the reorganization energy associated with the dominant intramolecular vibrational mode coupled to relaxation of the ^{3}MLCT excited state ($\lambda_M = S_M \cdot h\omega_M/2\pi$, where $h\omega_M/2\pi$ corresponds to the energy of that mode and S_M is the Huang–Rhys factor), and the full-width at half-maximum of the 0–0 vibronic component ($\Delta\bar{\nu}_{0,1/2}$). This latter term is related to the outer-sphere reorganization energy (λ_o) according to eq 7;

$$(\Delta\bar{\nu}_{0,1/2})^2 = (\Delta\bar{\nu}_{0,1/2}{}^0)^2 + 16(\ln 2)k_B\lambda_o T \qquad (7)$$

contributions from low-frequency modes of the chromophore that behave classically over the temperature range in question are also contained in this λ_o term. A plot of $(\Delta\bar{\nu}_{0,1/2})^2$ versus temperature (Figure 10) yields a value of 1355 cm^{-1} for λ_o. When combined with the average value of 1365 cm^{-1} for ω_M and a Huang–Rhys factor of $S_M = 0.99$, a total reorganization energy for ^{3}MLCT relaxation in [Zn$_2$(L)(mcb)(Ru((CF$_3$)$_2$-bpy)$_2$)]-(PF$_6$)$_3$ of ∼0.35 eV is indicated.

The contribution to the total reorganization energy from the acceptor will be limited to inner-sphere effects. Unfortunately, we have no direct information available concerning the structural changes associated with the formation of ligand-field excited state(s) in the dimanganese core of complex **4**. The relatively narrow bandwidths observed in the optical spectra of highly concentrated aqueous solutions of Mn(ClO$_4$)$_2$[62] implies that the Huang–Rhys factors associated with the ^{4}T$_{1g}$ and ^{4}T$_{2g}$ states of Mn^{II} are fairly small. Given this and the low frequencies characteristic of metal–ligand vibrational modes, we estimate that the acceptor contribution to λ is on the order of 0.1–0.2 eV, implying a total reorganization energy for Dexter transfer in complex **4** in the range of 0.4–0.5 eV. Plugging this result into eq 5 yields an electronic coupling constant of $H_{ab} \approx 0.15$ cm^{-1},[63] a small value but one that is qualitatively consistent with the remote nature of the excited state in this system.

[Mn$_2$(L)(mcb)(Ru((CH$_3$)$_2$-bpy)$_2$)](PF$_6$)$_3$ (3). Our current experimental setup does not allow us to collect subnanosecond time-resolved absorption data below room temperature, so we were unable to acquire a detailed temperature profile for the relaxation dynamics of [Mn$_2$(L)(mcb)(Ru((CH$_3$)$_2$-bpy)$_2$)](PF$_6$)$_3$ (**3**). Steady-state emission experiments were carried out on complex **3** dissolved in a 2:1 CH$_2$Cl$_2$/2-MeTHF mixture at 80 K. No emission was observed from the compound under these conditions, a result that argues against an electron-transfer mechanism.[45,58] The fact that the ^{3}MLCT excited state of complex **3** is localized directly adjacent to the Mn$^{II}_2$ core (i.e., the mcb$^-$ component of the charge-transfer state) coupled with the much smaller driving force for electron transfer ($\Delta G_0 = -0.1$ eV versus -0.43 eV for complex **4**) both point to a greater probability of Dexter transfer for this compound than for complex **4**. We are therefore reasonably confident that the photoreactivity of complex **3** is likewise defined by exchange
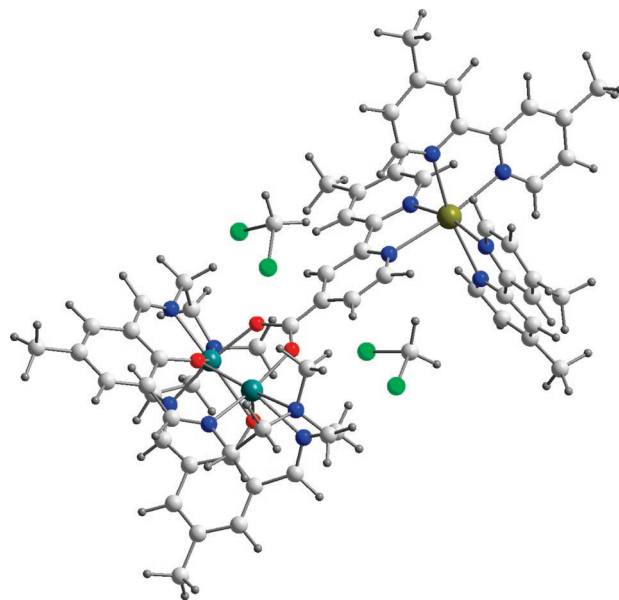

Figure 11. Molecular model of [Mn$_2$(L)(mcb)(Ru((CH$_3$)$_2$-bpy)$_2$)](PF$_6$)$_3$ (**3**), illustrating the possible interaction of two CH$_2$Cl$_2$ solvent molecules with the mcb bridge. The structure was created based on the known X-ray structures of the [Mn$_2$(L)(mcb)]$^+$ (Figure 1) and [Ru((CH$_3$)$_2$-bpy)$_2$(mcbEt)]$^{2+}$ components and performing a simple molecular mechanics minimization of the resulting assembly using SPARTAN.

energy transfer from the ^{3}MLCT excited state of the Ru^{II} chromophore to the Mn$^{II}_2$ core.

Proceeding under this assumption, we collected variable-temperature steady-state emission spectra for [Zn$_2$(L)(mcb)(Ru-((CH$_3$)$_2$-bpy)$_2$)](PF$_6$)$_3$ (**5**) (Figure S9) and performed a single-mode spectral fitting analysis in the same manner as described above for complex **6**. Not surprisingly, the results were quite similar overall to those obtained for the CF$_3$-substituted analog. The inner- and outer-sphere reorganization energies were determined to be 0.165 eV ($h\omega_M/2\pi = 1367$ cm^{-1} and $S_M = 0.977$) and 0.24 eV, respectively, indicating the total reorganization energy for relaxation of the ^{3}MLCT state is $\lambda \approx 0.4$ eV. The slightly larger value for the outer-sphere contribution in complex **5** relative to complex **6** is consistent with the qualitative appearance of the data as well as the fitting analysis indicating greater spectral narrowing with decreasing temperature than was observed for complex **6**; a small systematic increase in E_{00} was also noted.[64] Our expectation had been that the mcb-based excited state would be somewhat shielded from interactions with the solvent, thus leading to a smaller value for λ_o. Nevertheless, molecular modeling of complex **3** using SPARTAN[65] (Figure 11) does reveal an open cleft in the structure in the vicinity of the bridge that is large enough to allow solvent access to the bridge. We believe this is the likely origin of the increase in outer-sphere contributions to the ^{3}MLCT excited state.

Using the pre-exponential value of the Arrhenius term for complex **4** as the limiting reaction rate for the mcb-localized

(61) (a) Claude, J.-P.; Omberg, K. M.; Williams, D. S.; Meyer, T. J. *J. Phys. Chem. A* **2002**, *106*, 7795–7806. (b) Fleming, C. N.; Dupray, L. M.; Papanikolas, J. M.; Meyer, T. J. *J. Phys. Chem. A* **2002**, *106*, 2328–2334.

(62) Figgis, B. N.; Hitchman, M. A. *Ligand Field Theory and its Applications*; Wiley-VCH: New York, 2000.

(63) It should be noted that, due to the fact that H_{ab} is proportional to the fourth root power of both λ and temperature (eq 5), the magnitude of the coupling constant is relatively insensitive to either of these variables and is instead dominated by the value of k_0 as well the barrier reflected in exponential term in eq 2. With regard to the latter, the high density of acceptor states present in the Mn$^{II}_2$ core due to spin exchange between these ions makes coupling to state(s) that allow for a barrierless reaction pathway a reasonable assumption.

(64) The shift in E_{00} with decreasing temperature is related to the entropy change in the solvent according to $\partial E/\partial T \approx \Delta S_{lib}$, where ΔS_{lib} arises mainly from librational motion of the solvent due to excited-state decay (ref 32). For complex **5**, a plot of E_{00} versus temperature yielded a linear correlation ($R^2 = 0.986$) with a slope $\Delta S_{lib} \approx 2$ eu, a value that is roughly a factor of 2–3 smaller than what has been seen for isolated MLCT chromophores (e.g., the Re^I and Os^{II} complexes discussed in ref 32) but larger than what is seen for complex **6** ($\Delta S_{lib} \approx 0$). These results are consistent with the notion that solvent interaction with the ^{3}MLCT state in complex **5** is more substantial (thus leading to a larger value of λ_o) than in complex **6**.

(65) *SPARTAN, 5.0 ed.*; Wavefunction Inc.: Irvine, CA, 1997.

state and the value of λ obtained for complex **5**, we estimate $H_{ab} \sim 10$ cm^{-1} for complex **3**. This value, though admittedly not as well-determined as the one for complex **4**, nevertheless reflects in a reasonable way the expected change in H_{ab} between the Ru^{II} excited-state donor and Mn$^{II}_2$ acceptor upon bringing the pair in closer proximity.

Concluding Comments

We have presented an extensive analysis of the photoinduced dynamics of a donor–acceptor system in an effort to understand the mechanism responsible for its photoreactivity. The structural motif, consisting of a macrocyclic bimetallic core and an appended Ru^{II} polypyridyl complex, was designed in such a way as to allow for systematic modifications of the energetics and spatial characteristics of the excited state as well as provide for the preparation of suitable model complexes to aid in the interpretation of photophysical data. Both [Mn$_2$(L)(mcb)(Ru-((CH$_3$)$_2$-bpy)$_2$)](PF$_6$)$_3$ (**3**) and its fluorinated analog [Mn$_2$(L)-(mcb)(Ru((CF$_3$)$_2$-bpy)$_2$)](PF$_6$)$_3$ (**4**) exhibited significant quenching of their respective ^{3}MLCT excited states upon excitation of the Ru^{II}-based chromophore relative to the isostructural Zn$^{II}_2$ model complexes. Steady-state and time-resolved emission and absorption measurements carried out at room temperature were all consistent with Dexter transfer from the Ru^{II}-based excited state into the Mn$^{II}_2$ core; however, the driving force for back-electron-transfer coupled with differences in the spatial relationship between the donor and acceptor injected a degree of ambiguity into the problem such that a more detailed approach was needed.

Accordingly, variable-temperature steady-state and time-resolved measurements were carried out in order to quantify the reorganization energy associated with the photoreaction. In the case of [Mn$_2$(L)(mcb)(Ru((CF$_3$)$_2$-bpy)$_2$)](PF$_6$)$_3$ (**4**), the experimental data coupled with the known electron-transfer driving force of $\Delta G_0 = -0.43$ eV implies a reorganization energy that is too small to be associated with charge separation; this result in conjunction with the absence of any significant change in quenching dynamics upon formation of a low-temperature glass strongly supports an assignment of Dexter transfer for this system. A similar conclusion with regard to mechanism was reached for the methyl analog [Mn$_2$(L)(mcb)-(Ru((CH$_3$)$_2$-bpy)$_2$)](PF$_6$)$_3$ (**3**) based largely on the establishment of the mechanism in complex **4**, the smaller driving force for electron transfer ($\Delta G_0^{ET} = -0.1$ eV), and the fact that the donor/acceptor distance is much smaller in complex **3** due to

localization of the ^{3}MLCT excited state on the mcb bridge. Electronic coupling constants for Dexter transfer of $\sim$0.15 cm^{-1} and $\sim$10 cm^{-1} were estimated for complexes **4** and **3**, respectively, indicating that the shift in spatial proximity of the excited state from the periphery of the chromophore to the bridge linking the donor and acceptor translates to an increase in donor/acceptor coupling of nearly 2 orders of magnitude.

Distinguishing between Dexter transfer and an electron-transfer process in which the parameters governing charge-recombination are more favorable than the forward reaction represents a commonly encountered and sometimes intractable problem in excited-state chemistry. This ambiguity can arise quite easily in the photophysics of inorganic charge-transfer complexes in particular due to the energetics of the excited states involved. While the acquisition and interpretation of variable-temperature time-resolved data can be challenging, we believe this study demonstrates that the combination of such measurements along with suitable model complexes can help differentiate between these two mechanistic scenarios.

Supporting Information Available: Plots of the ESI-MS data for complexes **3**–**6** (Figure S1), electronic absorption spectra of complexes **1** and **2** (Figure S2), CV and DPV voltammograms of complex **3** (Figure S3), steady-state emission spectra for complexes **3** and **5** (Figure S4), variable-temperature time-resolved data for complexes **6** and **4** (Figures S5–S7), variable-temperature steady-state emission spectra for complexes **5** and **6** (Figures S8 and S9, respectively), and crystallographic data for complexes **1** and **2** in cif format. This material is available free of charge via the Internet at http://pubs.acs.org.

JA077096I